NASA/LARC JET PLUME RESEARCH

JOHN M. SEINER, MICHAEL K. PONTON, AND JAMES C. MANNING

NASA LANGLEY RESEARCH CENTER

HAMPTON, VA

FIRST ANNUAL

HIGH-SPEED RESEARCH WORKSHOP

MAY 14-16, 1991

SCOPE OF RESEARCH

The following provides a summary for research being conducted by NASA/LaRC and its contractors and grantees to develop jet engine noise suppression technology under the NASA High Speed Research (HSR) program for the High Speed Civil Transport (HSCT). The objective of this effort is to explore new innovative concepts for reducing noise to Federally mandated guidelines with minimum compromise on engine performance both in take-off and cruise. The research program is divided into four major technical areas as outlined below,

OUTLINE

A - JET NOISE RESEARCH ON ADVANCED NOZZLES

1 - LANGLEY AXISYMMETRIC MIXED FLOW NOZZLE
2 - PRATT & WHITNEY 2-D HYPERMIX NOZZLE
3 - HIGH TEMPERATURE EJECTOR LINERS
4 - BOEING NACA NOZZLE
5 - LANGLEY FORWARD FLIGHT SIMULATOR
6 - LDV AND WATER COOLED PROBE DEVELOPMENTS

B - PLUME PREDICTION AND VALIDATION

1 - EVALUATION OF RNS TO BASELINE AXISYMMETRIC JETS
2 - AXISYMMETRIC PLUG VALIDATION EXPERIMENT
3 - EVALUATION OF COMPRESSIBLE TURBULENCE MODELS
4 - SHOCK/VORTEX INTERACTION STUDY

C - PASSIVE AND ACTIVE CONTROL

1 - NOZZLE GEOMETRY EFFECTS
2 - MULTIPLE JET INTERACTIONS
3 - CURVED JET MIXING
4 - ACTIVE CONTROL OF INITIAL JET SHEAR LAYER

D - METHODOLOGY FOR NOISE PREDICTION

1 - SUPERSONIC INSTABILITY WAVES
2 - NON-LINEAR WAVE INTERACTIONS
3 - COMPRESSIBLE RAYLEIGH EQUATION DEVELOPMENT
4 - PREDICTION OF NOISE FOR NON-ROUND JET GEOMETRY
5 - LOW REYNOLDS NUMBER RESEARCH

A1 - LANGLEY AXISYMMETRIC MIXED FLOW NOZZLE

A dual co-annular stream axisymmetric nozzle has been designed (figure 1a) and fabricated (figure 1b) to support HSR. The model was designed with removable contour parts at the nozzle exit to accommodate a wide range of geometries for concept investigations, including conversion to single stream configurations. These removable parts are fabricated from Haynes 230 alloy, which along with water cooling of the non-removable stainless steel nozzle duct, permits testing the model to 2500°R. Depending on the nozzle geometry selected, the mixed flow model scale size to full was designed to be between eight and ten to one.

The Jet Noise Laboratory (JNL) at Langley can supply two independently controlled air streams (25 lbm./sec. each) to power the mixed flow model. The outer stream is supplied by a Marquart sudden expansion propane/air fueled burner, which enables testing to the 2500°R temperature limit of the model at a nozzle pressure ratio of 10.5. Air supplied to the propane burner is pre-heated electrically to improve combustor stability. The inner stream is electrically heated (500 KW), enabling testing to 1460°R with 2 lbm./sec. air to a nozzle pressure ratio of 10.5. Both inner and outer flow stream air, fuel, electrical heat, and water system are remotely controlled using a distributive process system controller.

The design of a two dimensional mixed flow nozzle system, like that shown in figure 1a, is currently in progress.

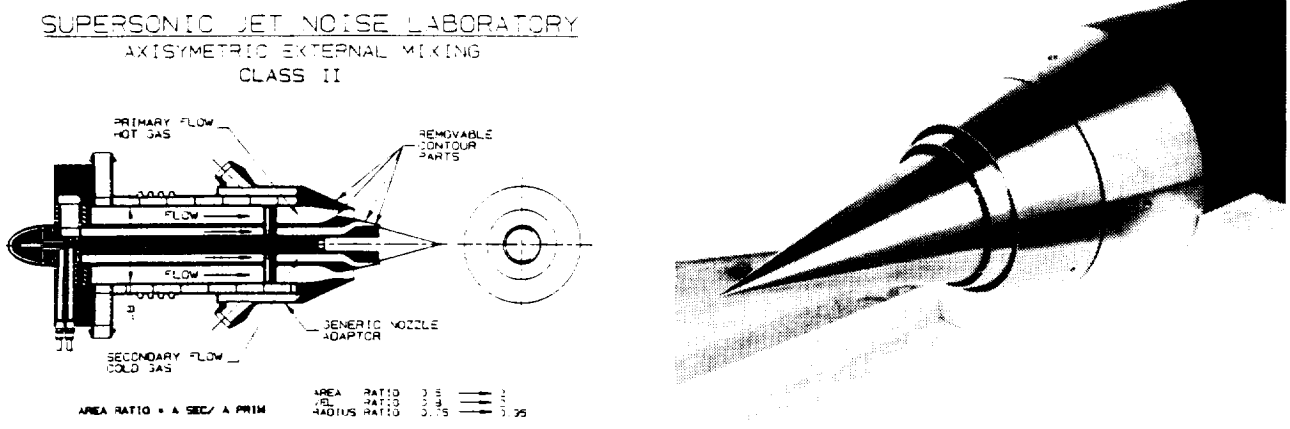

a - schematic of dual stream nozzle design concept.

b - photograph of high radius ratio mixed flow nozzle.

Figure 1. Langley mixed flow axisymmetric nozzle with removable high temperature alloy nozzle parts.

A2 - PRATT & WHITNEY 2-D HYPERMIX NOZZLE

A sharp focus schlieren apparatus with imaging radiometer is being developed at Langley to provide flow visualization for diagnostic evaluation of individual mixer elements of the Pratt & Whitney 2-D mixer ejector nozzle. This nozzle is scheduled for test later this year in the NASA Lewis 9 X 15 foot wind tunnel.

As shown in figure 2, the model contains four mixer lobes. These lobes were designed as convergent-divergent passages to minimize shock noise. High temperature air (2000°R) is ducted from the NASA/Lewis hydrogen/air fueled propulsion model through these mixer lobes. In addition to the noise reduction produced by mass flow augmentation by the ejector, the model additionally reduces noise through the creation of large scale axial vorticity on the nozzle afterbody. The large scale vorticity accelerates mixing of external air with hot flow from the lobes, thereby reducing flow velocity and noise.

The flow visualization experiments will enable interpretation of noise reduction to the flow physics inside the ejector. Figure 3 provides a schematic for the sharp focus schlieren apparatus being assembled for the NASA/Lewis tunnel. The designed of this apparatus is based on the methods developed by Weinstein (1991). The optical axis is vertical. The ejector's flat sidewalls will be replaced with a set having optical viewports. The optical glass is Infrasil 302, which transmits in the infra-red to 3.2 microns. This glass can be ground to achieve schlieren quality. A double pulsed ND-YAG laser with 35 mJ output in the green (532 nm) is the light source. This laser can be fired as a single shot laser or synchronized externally at 30 Hz. to a video camera. The laser's pulse duration is 7 nsec, thus allowing instantaneous view of flow features.

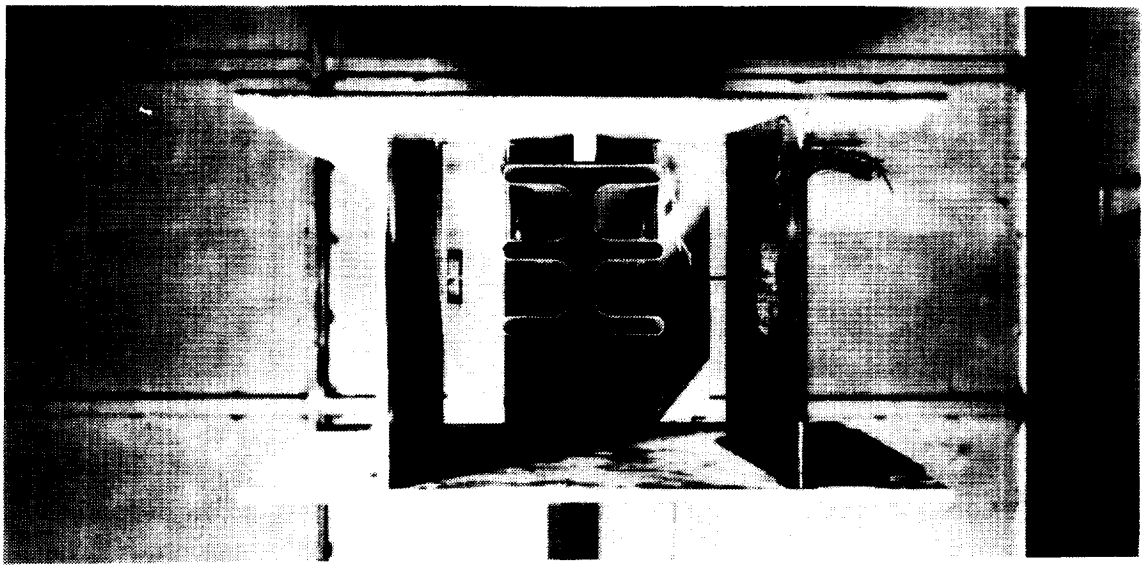

Figure 2. Pratt & Whitney 2-D mixer ejector nozzle in NASA/Lewis 9 X 15

A2 - APPLICATION OF SHARP FOCUSED SCHLIEREN

Flush mounted optical windows are being constructed for both the tunnel floor and ceiling. The 20" X 24" crown glass floor window contains the first schlieren grid and fresnel lens. The ceiling window is Infrasil 302. A f/3.6 lens with 6" clear aperture is mounted behind the ceiling window. Based on the fixed distances of the model in the tunnel and the optical aperture through the model, the f/3.6 lens was selected to produce a sharp focus less than the 0.4 inch mixer lobe thickness. Flow features beyond 1.25 inches cannot be distinguished with this apparatus. This means that the schlieren apparatus will be able to isolate flow details from a single mixer lobe. A rigid support mounted to the tunnel ceiling is used to support the second schlieren grid, image plane viewfinder, 70 mm film and video camera.

Radiometric measurements with a dual imaging radiometer will be conducted using the same optical access ports. The radiometer contains a narrow band filter centered at 2.6 microns to enable imaging of water produced as a by-product of combustion between hydrogen and air. Because the radiometer's depth of focus exceeds that of the model width, it will be necessary to seed a given mixer lobe with CO_2. Since CO_2 emits at 4.2 microns, both the model and ceiling windows will be replaced with sapphire to conduct these tests. The radiometer is equipped with a narrow band filter around 4.2 microns. Using this method, the mixing of a single mixer lobe can be traced.

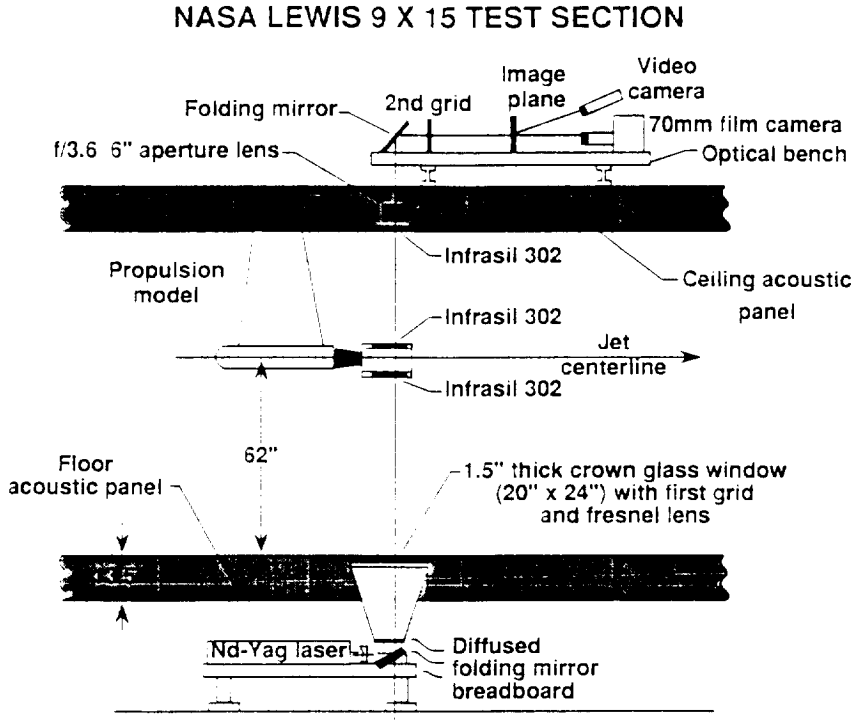

Figure 3. Schematic of sharp focus schlieren apparatus for NASA/Lewis test of P & W nozzle.

A3 - HIGH TEMPERATURE EJECTOR LINERS

Application of acoustic treatment to mixer ejector walls has been proposed as a method to achieve additional noise reduction. Both P & W, GEAE, and Boeing have used ejector liners in previous suppressor nozzle studies, achieving varying degrees of success. These liners have typically been fabricated using a bulk absorber with perforated face sheet. Little is known about the effectiveness of such a concept in the presence of distributed broadband sources, whose locations and frequencies depend on the mixer suppressor geometry. Temperature gradients and high speed grazing flow with shocks provide a formidable challenge to existing liner technology.

NASA Langley has begun an investigation of acoustic liners for the HSCT. The study will use the JNL to study candidate materials in the presence of high speed and high temperature grazing flows. In parallel efforts to this effort, T.L. Parrott, of the Langley Applied Acoustics Branch, will develop candidate materials for these studies using a flow impedance tube, and Gary Settles of Penn State Univ. will evaluate the aerodynamic performance of these candidate materials.

The JNL studies will initially begin by using a small 2-D C-D 1460°R Mach 2 rectangular nozzle with ejector, as shown in figure 4a. The sidewalls of the ejector are adjustable. The construction of this model is complete. The aspect ratio of the nozzle is 7.2 to simulate two dimensional wave emission. The sidewalls of the ejector contain optical viewports to permit flow visualization. For large plume/wall separations, it is possible to identify the emitted Mach wave angle to the impedance boundary, provided no acoustic interaction occurs between the plume and duct modes. This is illustrated in figure 4b, which provides indication that in-situ measurements of material impedance will also be determined. For small plume/wall separations the aerodynamic boundary layer over the liner face sheet can be visualized. Both aerodynamic flow measurements and far field acoustic measurements (ejector treated on four walls) will be conducted to support this research.

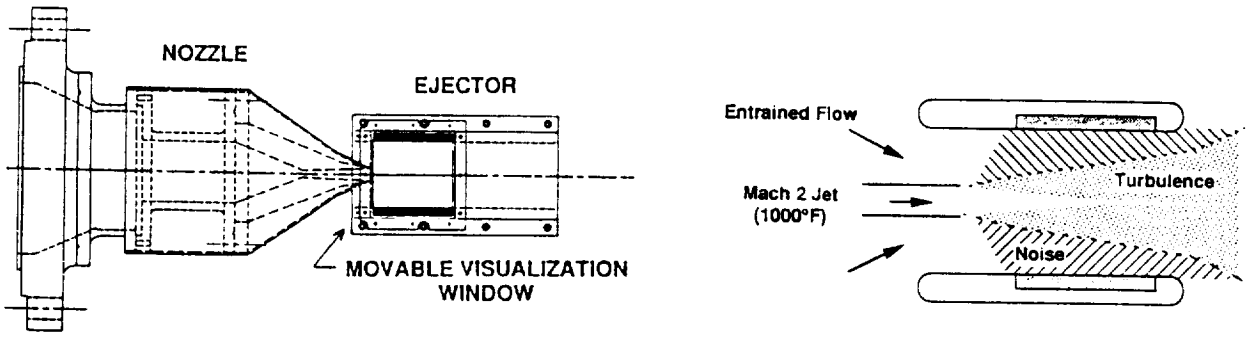

a - model hardware **b** - experimental setup

Figure 4. Initial JNL study of acoustic liners for HSCT ejectors.

A3 - HIGH TEMPERATURE EJECTOR LINERS

The upper and lower walls of the ejector will be lined with various length and depth candidate materials being developed in the Flow Impedance Tube Laboratory (FITL). Early concepts to be studied in the JNL include investigation of ceramic honeycomb material with small diameter cells, whose absorption is dominated by viscous dissipation. Such materials are aerodynamically smooth and do not require a face sheet. Such smoothness does, however, bring into question liner absorption capabilities at high angles of grazing incidence. To achieve broadband absorption characteristics using ceramic honeycomb, both stepped and variable depth liners will be investigated. A broadband liner material, Permablique (figure 5), will also be investigated. In addition to the ceramic honeycomb, bulk liners using Kevlar with perforated face sheets will be investigated to provide comparison to industry experience.

In the JNL, in-situ measurements of impedance will be conducted using water cooled pressure transducers. This technology has been successfully developed to enable measurement of dynamic pressure in high temperature environments, as indicated in figure 6. To apply this technology to the liner program will, however, require an investigation of the phase characteristics of piezorestive transducers. Similar measurements will be performed in FITL, with eventual development of a theoretical model to describe absorption behavior.

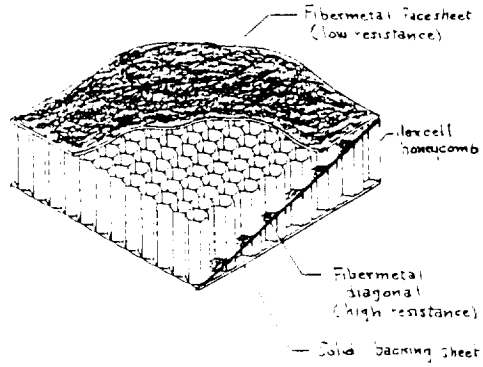

Figure 5. Permablique, a locally reacting acoustic liner with spatially dependent frequency tuning.

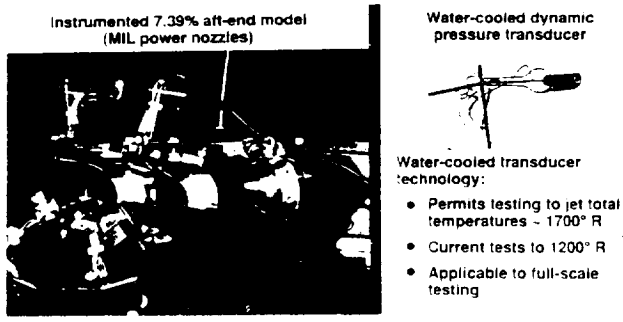

Figure 6. Water cooled piezorestive transducer for high temperature flow.

A4 - BOEING NACA NOZZLE

In a joint effort with Boeing, a flow visualization investigation of the Boeing NACA nozzle series was conducted in their LSAF by the Langley JNL staff. The objective of the Langley effort was to assist Boeing with analysis of the aeroacoustic data, primarily through acquisition of flowfield data. For these tests both a conventional schlieren system and imaging radiometer were used for flow visualization. Figure 7a shows the NACA nozzle mounted in the Boeing LSAF. Both the imaging radiometer and linear array are visible in this figure.

The naturally aspirated coannular (NACA) nozzle of Boeing is shown schematically in figure 7b. Supersonic hot exhaust air from the turbine is ducted to the outside duct of the nozzle. The outer stream shroud could translate, thus providing an outer stream with adjustable area ratio. Subsonic secondary air is entrained through the ejector and ducted to the inner stream. The secondary air is augmented by air bypassed from the turbine stage, since an HSCT engine should have margin at take-off. The secondary air stream is unheated and subsonic. Acoustically, the scaled NACA nozzle achieved between 9 and 10 EPNdB of suppression with little performance penalty.

The conventional schlieren apparatus utilized a 100 nsec 10 kHz spark source with capability of being fired externally to obtain conditionally sampled data. A video camera was used to record data and post processed using image analysis software. The most difficult part of the set-up involved folding the optical axis with a mirror located in the upper left hand corner of the forward flight nozzle. This requirement arises in LSAF due to the proximity of the nozzle and forward flight nozzle to a wall.

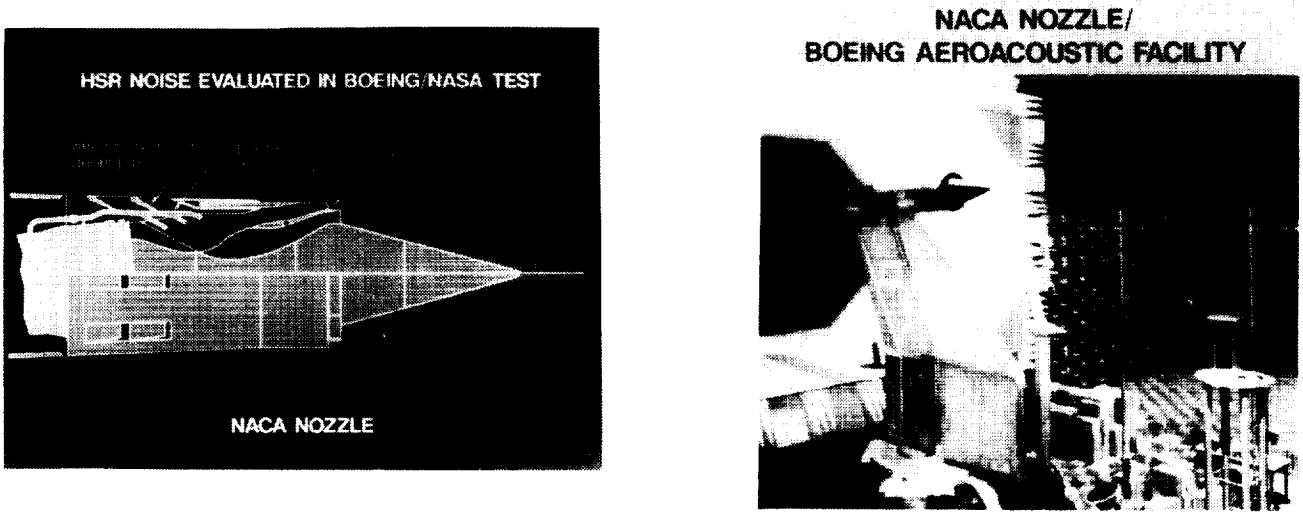

a - schematic of NACA nozzle **b** - NACA nozzle mounted in LSAF

Figure 7. Boeing NACA nozzle flow visualization study.

A4 - NACA NOZZLE SCHLIEREN DATA

With the schlieren data, it was possible to determine the optimum location for shock free flow. This was determined to occur at the translating shroud position L_s = -0.5". The optimum shroud location was found to be dependent on forward flight Mach number and turbine bypass flow. Example schlieren results obtained with NACA 2.3 are shown in figure 8. As can be observed, in addition to changes in shock structure, the shear layer spread rate is very dependent on operational parameters of the nozzle.

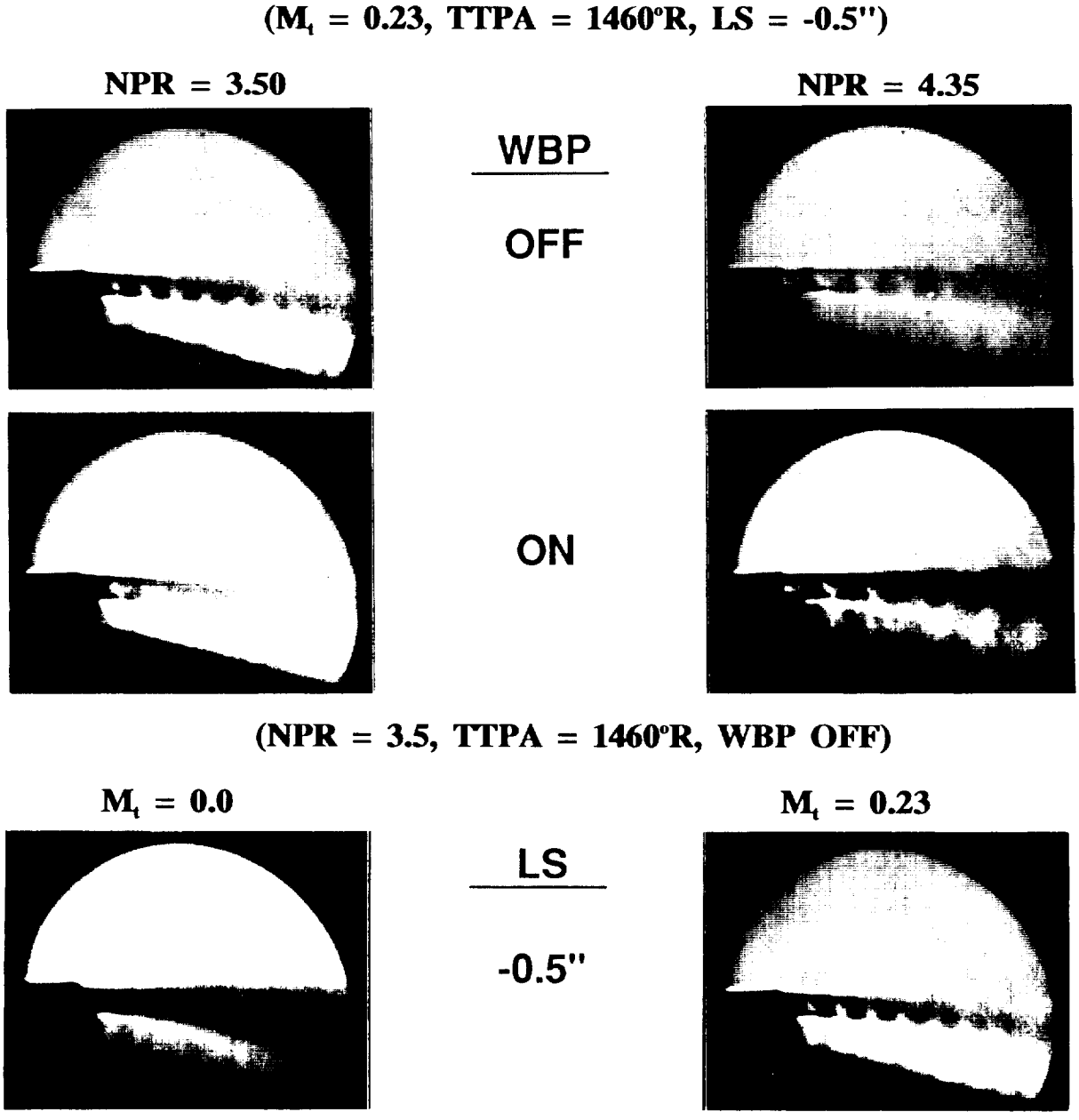

Figure 8. Schlieren data from NACA nozzle study.

A4 - NACA NOZZLE RADIOMETRIC DATA

The imaging radiometer used in this study proved valuable in providing information on the flow uniformity of the model and post merged regions of the flow. The radiometer was capable of simultaneously imaging radiation between 8 and 12 microns through one channel, and 4.2 microns through a second channel with narrow band filter. The long wavelength channel is used to image metallics associated with the nozzle, while the short wavelength is used to image CO_2, a by-product of the propane air combustion. Figure 9 shows the degree of flow non-uniformity (later traced to unsymmetric flow in combustor) and the enhanced mixing produced by application of the turbine bypass flow. These results, which represent an average of 100 consecutive frames, were obtained for NPR = 3.5, TTPA = 1460°R, and LS = -0.5".

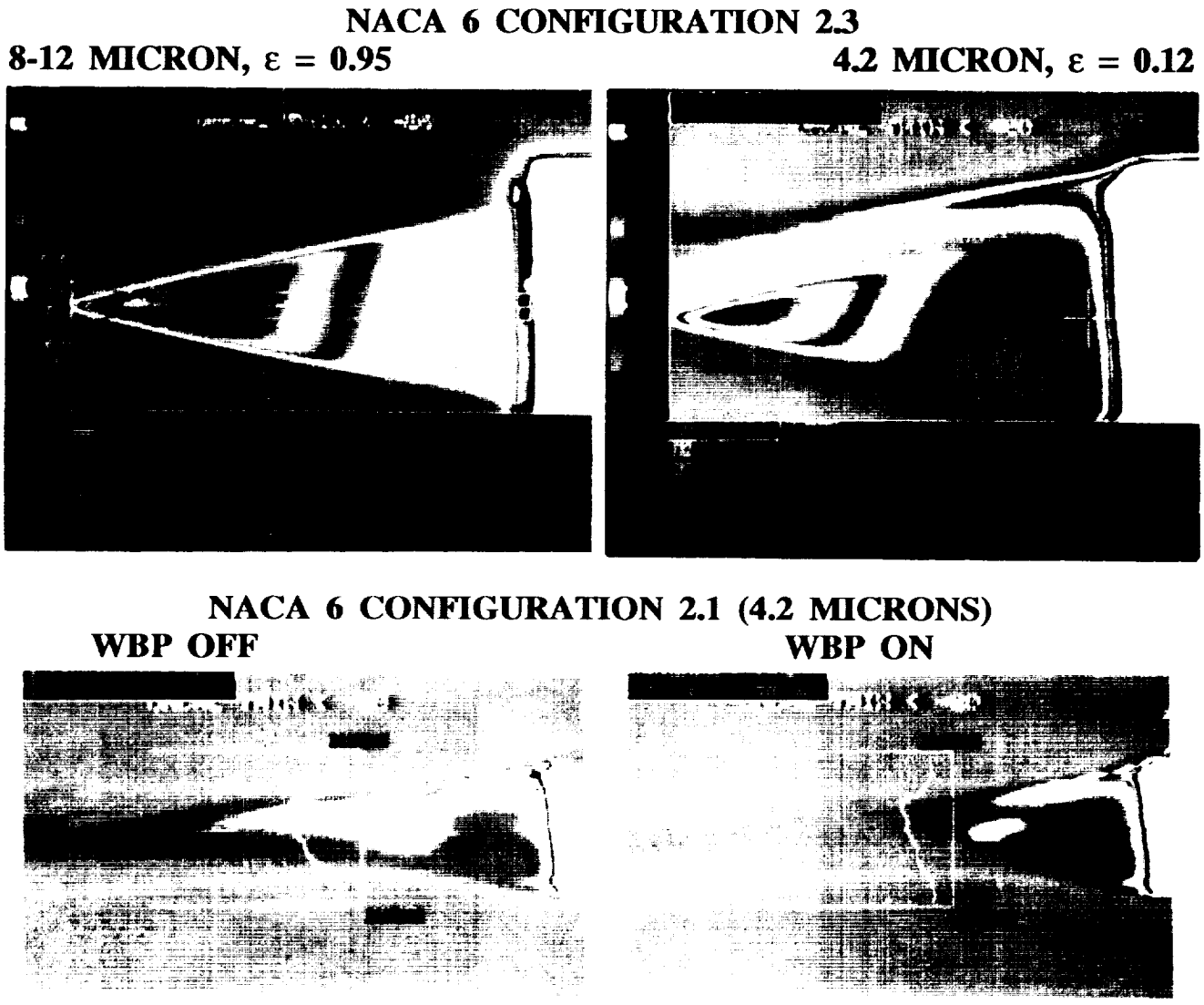

Figure 9. NACA nozzle dual wavelength band radiometric results.

A5 - LANGLEY FORWARD FLIGHT SIMULATOR

A forward flight simulator with propulsion model is currently being designed on a FY-92 CoF for installation in the NASA/LaRC Jet Noise Laboratory. The simulator and propulsion model will complete all facility requirements necessary for HSCT research in the take-off mode. Figure 10 provides a schematic of the proposed forward flight system and propulsion model.

The tunnel is powered by a 10 ft. diameter two stage axial flow fan that is driven by a variable speed drive with a 4000 HP motor. The fan is capable of pulling 50" H_2O at 420,000 CFM. With a 4 X 5 foot nozzle exit, this corresponds to a forward flight simulation velocity of 350 ft./sec. The area contraction ratio of the nozzle is 11.25. The nozzle inlet duct entrance is equipped with a honeycomb flow straighter and six continuously woven wire mesh screens. The anechoic test section is 36 X 18 X 18 ft., wedge tip to wedge tip. The first diffuser utilizes a 2.5 degree half angle with a 5 X 5 ft. throat. A collector is used to help recovery of the free jet static pressure. A second diffuser, of 3° half angle, is used to slow the flow for the final duct silencer.

The propulsion model will have similar features to existing JNL nozzle hardware, allowing existing nozzle parts to be utilized. The model will house a burner capable of heating 10 lbm./sec of air to 2460°R. The primary mode of combustion will be propane/air, with capability of operating from a hydrogen/air supply. A single component balance will be installed for rudimentary performance assessments.

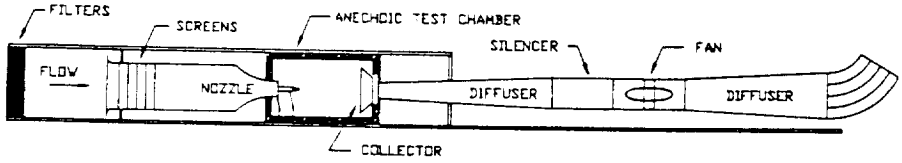

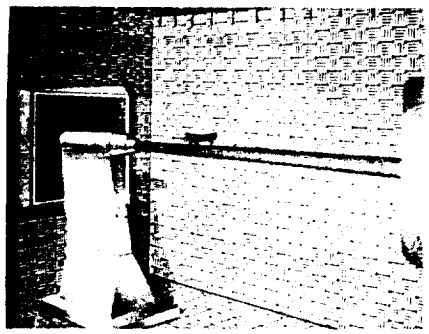

PROPANE/AIR FUELED COMBUSTOR

T_{max} = 2500°R

Q = 420,000 CFM @ 50" WATER

V_{max} = 350 FT./SEC.

Figure 10. NASA/LaRC Jet Noise Laboratory Forward Flight Simulator.

A6 - JNL LASER VELOCIMETER SYSTEM

The JNL laser Doppler velocimeter is capable of measuring 2 velocity components. A schematic of the system is shown in figure 11a. The system is based on a fiber optic LDV probe which allows the 15 watt argon-ion laser to be located remotely (25 meters) from the test chamber so that it is not subject to high intense noise fields. Figure 11b shows the now obsolete single axis fiber optic system mounted in the test chamber. The probe's nominal dimensions of 3" diameter by 18" long. make the probe easily mountable on the Laboratory's 3 axis digital probe traverse mechanism. At the laser end of the probe, there are four fiber ends for laser beam transmission to the jet test cell. Two transmit 514.5 nm and two transmit 488.0 nm. The optical components at the laser site allow for color separation, beam splitting, and frequency shifting before transmission through the optical fibers. In the test chamber, a lens is mounted with a focal length of 600 mm., which will produce a minimum of 20 good fringes. The light scattered by seed particles entering the probe volume are collected in the off-axis backscatter mode. Six inch diameter collection optics are mounted on a movable platform that allows the backscatter angle to be optimized for maximum signal strength. Off-axis backscatter is generally superior for collecting light from small seed particles. The seed particles used in the JNL for hot flows are alumina powders with nominal particle size of 0.3 microns. Particles are injected into the air supply line with a fluidized bed seeder operated from the control room.

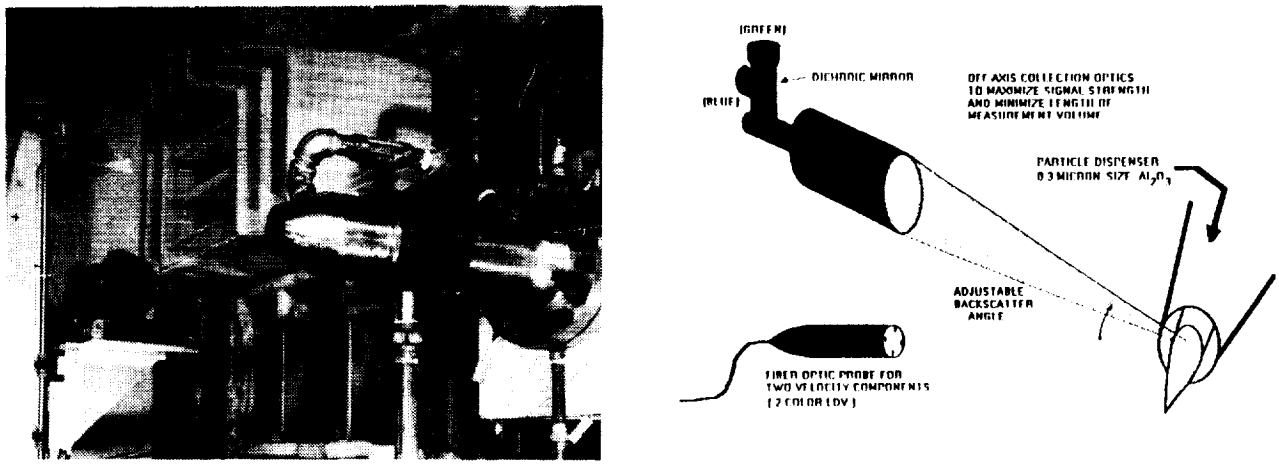

a - schematic of JNL 2-color LDV **b** - single component LDV in JNTC

Figure 11. Description of JNL laser velocimetry system.

A6 - JNL WATER COOLED PROBE DEVELOPMENTS

Three types of water cooled supersonic probes were developed and tested to study high temperature jet plumes. The probe types include total temperature and total and static pressure. All probes were designed with a diameter of 4.76 mm and a wall thickness of 0.38 mm. An annular coolant system was utilized for all three designs, and proved satisfactory to temperatures of 2460°R in Mach 2 flow. A three dimensional cut-away view of the static pressure probe is shown in figure 12. A single center tube, proceeding up to the backside of the tip, provides coolant water to the probe. The water sprays the back of the tip, and symmetrically immerses the region between the inlet water tube and inner wall of the probe as it proceeds to the probe aft. Four tubes inside the probe serve to read the average static pressure. The shape of the exterior probe geometry matches that previously used with uncooled probes in the JNL. The total pressure probe, not shown, is designed by similar methods. The total temperature probe incorporated the annular cooling up to a region near the thermocouple bead as shown in figure 13. The thermocouple bead is located in a blackbody cavity and samples high temperature air, whose velocity is controlled by the probe inlet and exit ports. The area ratio of inlet to exit ports are selected to produce subsonic flow over the thermocouple bead. A portion of the thermocouple sheath forms a liquid tight seal between the test and coolant chambers.

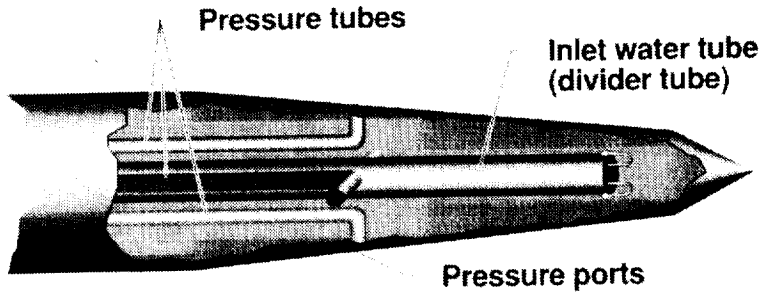

Figure 12. Illustrated cut-away view of cooled static pressure probe.

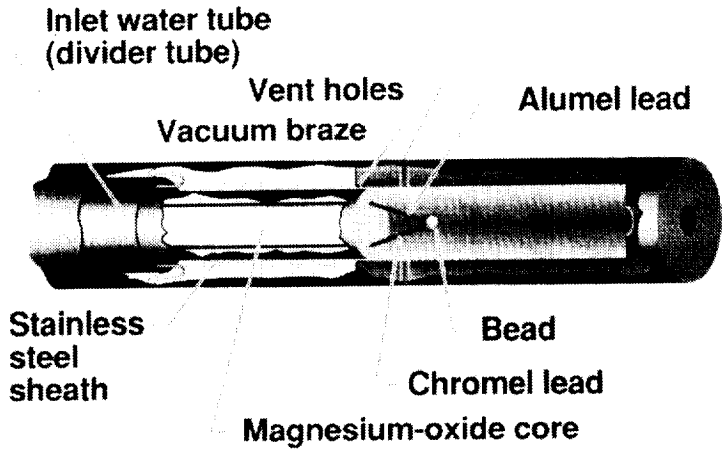

Figure 13. Cut-away view of cooled total temperature probe tip.

A6 - JNL WATER COOLED PROBE DEVELOPMENTS

The data obtained from the total and static pressure probes were found satisfactory to temperatures of 2460°R in Mach 2 flow. The data from the water cooled temperature probe, however, was affected by the water coolant. This required the development of a phenomenological model for heat transfer to the thermocouple bead to account for heat transferred to the coolant. The rate of heat transfer to the TC junction was found, for example, significantly higher with water coolant activated.

The heat transfer analysis developed a relationship between the indicated probe bead temperature and freestream flow total temperature. This analysis solves a heat balance equation involving radiative, convective and conductive modes at the TC junction. The accuracy of this relationship is shown in figure 14, which compares indicated and corrected bead temperatures. The indicated bead temperature is represented by the triangular and circular points. The circular points represent data obtained at jet plume locations with known local total temperature, whereas the triangular points represent data at unknown local jet total temperatures. Comparison of the circular and triangular data points shows the degree of departure from ideal response. The three known data points were used to obtain coefficients for the heat transfer analysis. Application of the model analysis, produces corrected temperatures that appear to be in satisfactory agreement to the known jet total temperature. This is indicated by the square data points.

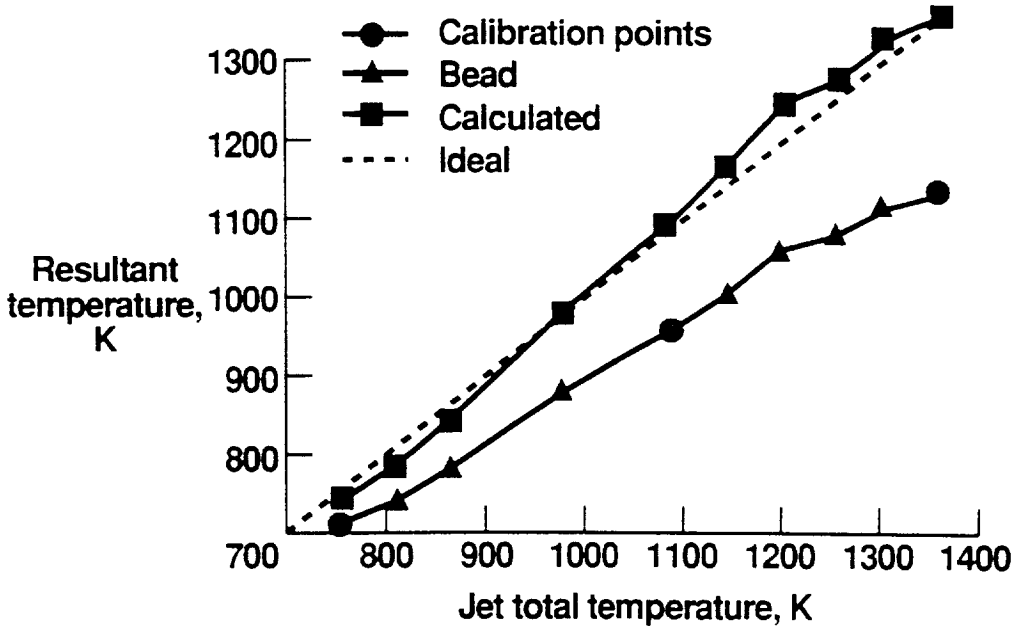

Figure 14. Calculated total temperature compared to indicated bead temperature for variuos jet centerline temperatures.

B1 - EVALUATION OF RNS TO BASELINE AXISYMMETRIC JETS

Numerical prediction of jet plume structure provides support for theoretical and empirical based jet noise prediction methods. For extremely complex nozzle geometry, like that of an HSCT suppressor nozzle, CFD prediction of flow structure is essential. Prior application of the PNS code SCIPVIS to a Mach 2 underexpanded axisymmetric jet provided satisfactory agreement to measured data as shown in the plume static pressure variations of figure 10. In this example, SCIPVIS is using the kW two equation turbulence model. These results are encouraging, however, several important deficiencies exist in applying PNS to more complex jet flows.

The PNS cannot handle non-uniform subsonic external flow, large Mach discs, multiple jets, or large scale 3D vortical behavior. All these are important in application to HSCT. Even for the simple axisymmetric jet, it is remarkable that the PNS could achieve such good success, since it neglects all streamwise stress/diffusive terms. In a recent study, SAIC finds that neglect of the streamwise terms actually produce errors that are compensated by those introduced by the simplified treatment of the subsonic portion of the shear layer. Their results show that pressure variations in the subsonic layer, which are produced by shock/shear layer interactions, influence the upstream development of the flow.

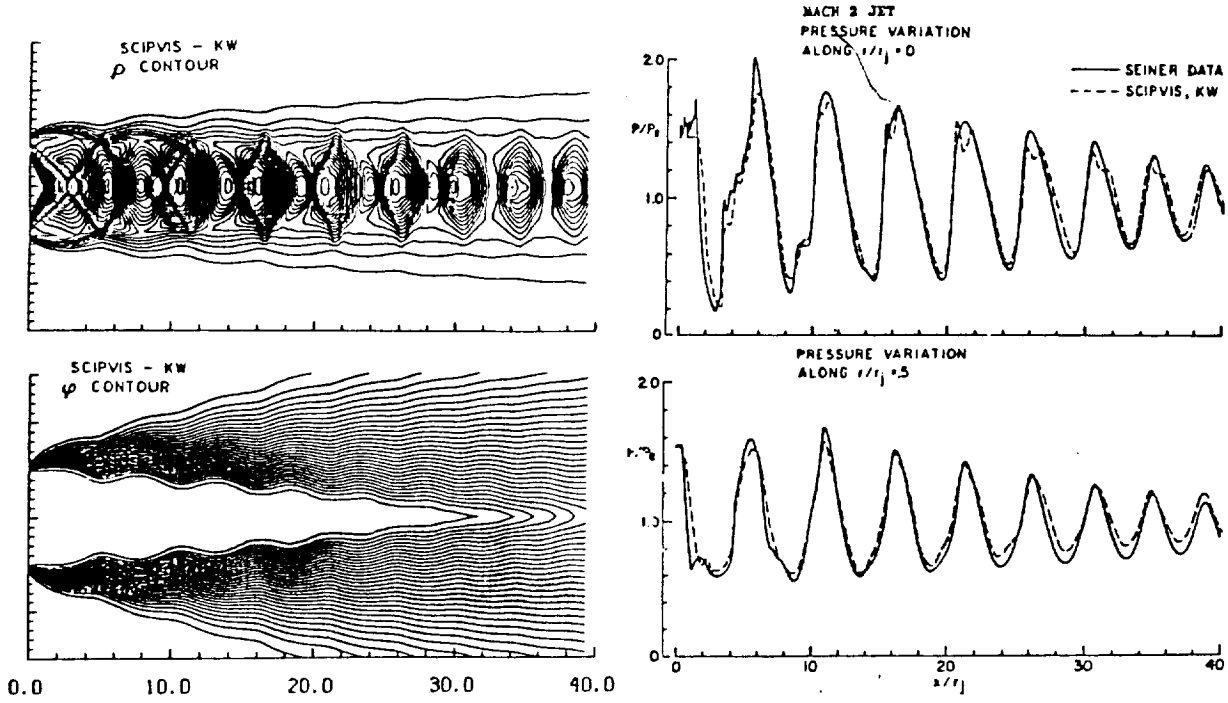

Figure 15. PNS prediction of Mach 2 underexpanded jet with kW model.

B1 - EVALUATION OF RNS TO BASELINE AXISYMMETRIC JETS

In the SAIC investigation of the Mach 2 underexpanded axisymmetric jet, two RNS (Reynolds Averaged Navier-Stokes) codes, PARCH and CRAFT, were studied using the **kε** turbulence model. The SCIPVIS code with **kε** was used as a benchmark. The PARCH code uses an implicit central-differencing Beam-Warming algorithm to solve the full Navier-Stokes equations. The PARCH code contains blocking and complex griding schemes that make it attractive for use with complex nozzle geometry. The CRAFT code is finite volume with upwind numerics. Figure 11 shows a comparison between all three codes in their prediction of the jet static pressure and total enthalpy along the centerline of the Mach 2 underexpanded jet plume. As can be observed, even though both RNS and PNS exhibit the same rate of mixing, substantial differences exist between the codes with regard to wave attenuation beyond the second shock cell. The CRAFT code produces less wave attenuation than PARCH, but both RNS codes show significant wave attenuation relative to PNS.

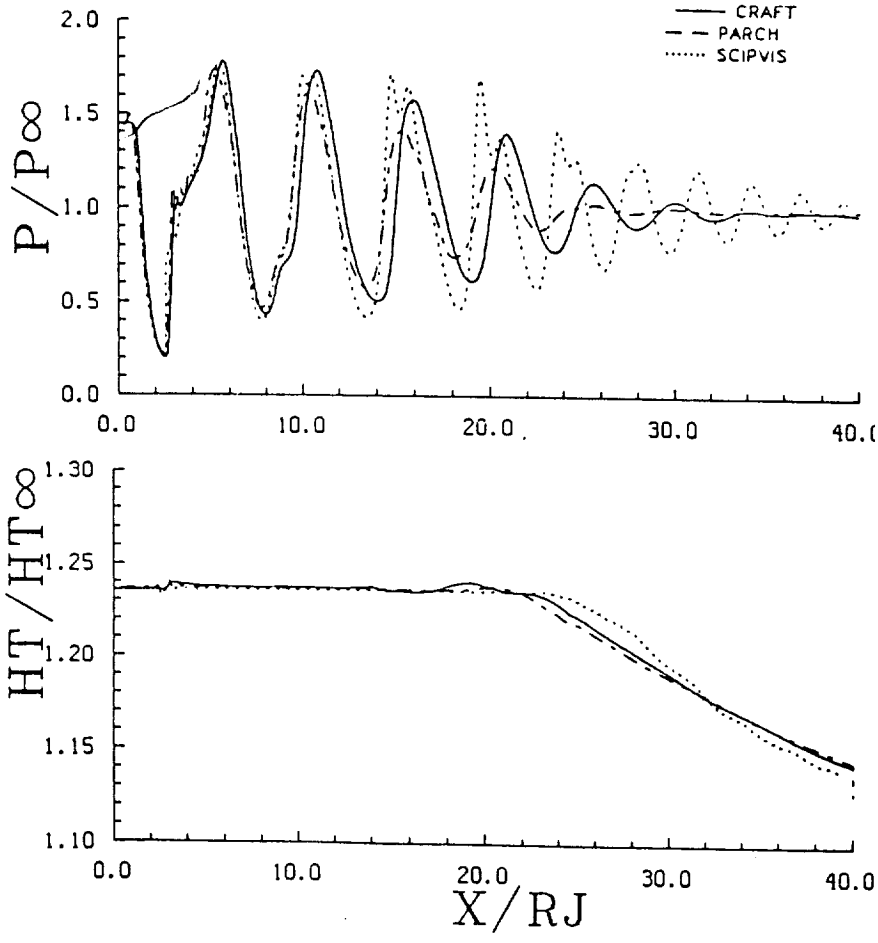

Figure 16. Comparison of PNS and RNS prediction of Mach 2 jet.

B1 - EVALUATION OF RNS TO BASELINE AXISYMMETRIC JETS

In an attempt to understand the mechanism for wave damping, SAIC first compared the performance of all three codes using laminar calculations with thin shear layer. The results showed that all three codes predicted the same overall shock structure, the CRAFT code showing the smallest level of numerical dissipation. As a final step, numerical calculations were made using the PARCH code with the full stress tensor retained and with the streamwise viscous/diffusive terms dropped. As can be observed in figure 12, this has a profound influence on wave damping. Retention of the full stress tensor leads to significant damping of the wave structure beyond the third shock cell. This suggests that the turbulence model used in the calculation is critical to achieving a satisfactory prediction for plume shock structure. Thus at this point more research is required on these 3D RNS codes before they can be reliably used to assist in a shock noise calculation.

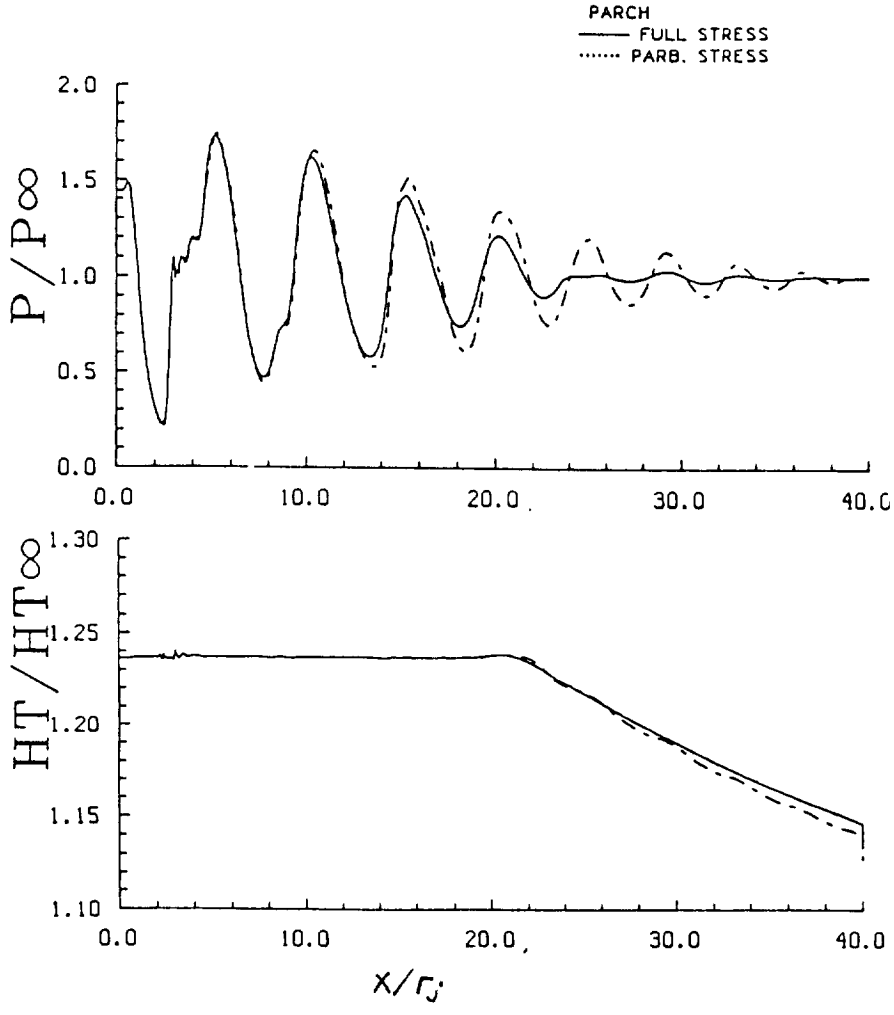

Figure 17. Effect of streamwise viscous/diffusive terms on wave damping.

B2 - AXISYMMETRIC PLUG VALIDATION EXPERIMENT

The axisymmetric plug nozzle represents a good candidate for validation of CFD for HSCT applications. The internal boundary and large wall curvature are all features that can be associated with a complex suppressor nozzle configuration. The nozzle design area ratio is equivalent to Mach 1.5 at 2060°R. For the present numerical/experimental program a plug half angle of 15° is initially being considered. The plug contains ventilation for boundary layer control to prevent separation and for shock management. The geometry of the wall ports are selected to minimize noise. The degree of ventilation can be controlled. Figure 11 illustrates the nozzle geometry. A removable hatch is used to enable installation of various plug surface measuring devices. The plug is being manufactured to include an non-instrumented and non-ventilated plugs. The measurement methodologies to be utilized are as follows:

Plug Body	PLUME	ACOUSTICS
STATIC WALL PRESSURES	TOTAL & STATIC PRESSURE	FAR FIELD LINEAR ARRAY
DYNAMIC WALL PRESSURE	MEAN VELOCITY (LDV)	NEAR FIELD CONTOURS
SURFACE TEMPERATURE	REYNOLDS STRESS (LDV)	SOURCE LOCATION
HEAT TRANSFER MEAS.	TOTAL TEMPERATURE CONTOURS	
WALL SHEAR STRESS	STATIC TEMPERATURE MEAS.	
PLUG VENTILATION	FLOW VISUALIZATION	

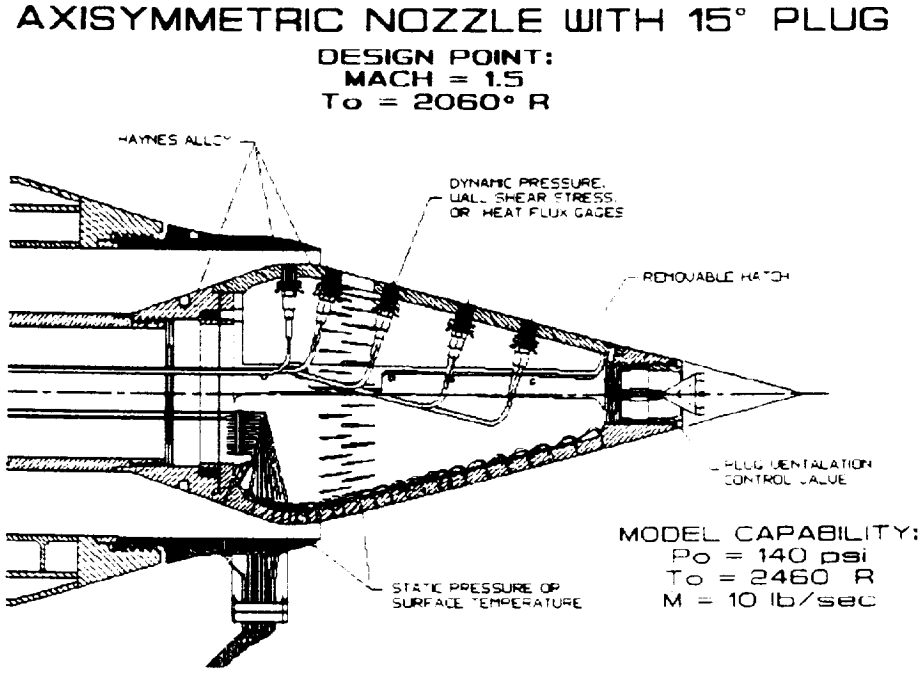

Figure 18. Single stream axisymmetric plug flow nozzle for validation experiment.

B2 - AXISYMMETRIC PLUG PARCH CODE RESULTS

Initial calculations have been performed at SAIC using PARCH for the axisymmetric plug nozzle geometry described above. In a parallel effort, Nick Georgiadis of NASA Lewis has applied the PARC code using the same nozzle geometry. For the work at SAIC, a full Navier-Stokes analysis is applied to determine slip wall versus no slip wall behavior. The flow calculation begins internal to the nozzle, where a 91 X 71 adaptive grid is used to compute internal flow. The Chien low Reynolds number $k\varepsilon$ turbulence model is used to enable calculation into the wall region. The PARCH code predicts transition to occur inside the nozzle duct. The plug jet adaptive grid consisted of a 201 streamwise by 101 crossstream mesh. The analysis assumes an adiabatic wall. In the experimental model, heat flux measurements will be conducted using specially designed calorimeters to aid the numerical analysis.

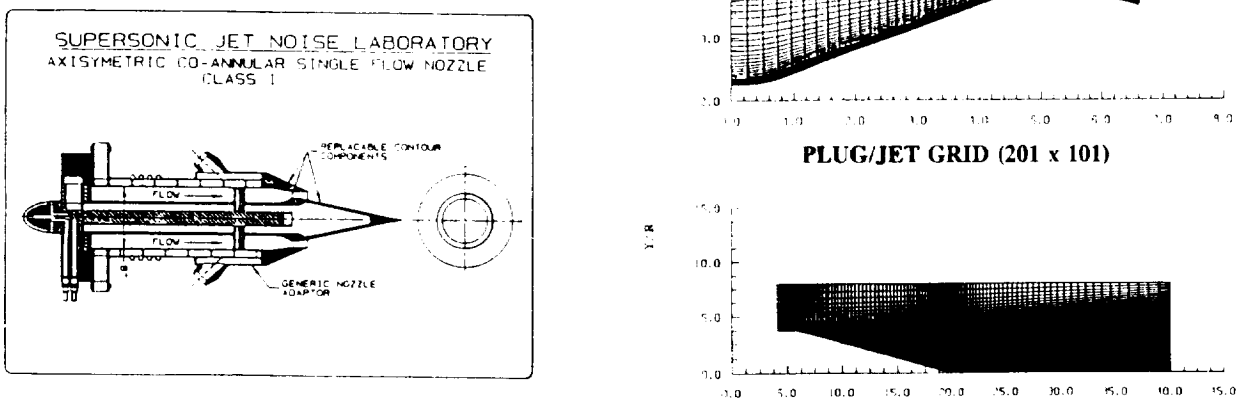

Figure 19. Parch code adaptive grid for axisymmetric plug nozzle.

B2 - AXISYMMETRIC PLUG PARCH CODE RESULTS

Figure 15a compares static pressure results between the slip and non-slip wall. As can be observed significant attenuation of shock/wave structure occurs due to interaction with the turbulent plug boundary layer. The numerical simulation involves operation of the nozzle at its design pressure and temperature ratios. On exiting the nozzle, both the slip and non-slip solutions accelerate the flow beyond the nozzle design point. The nozzle exit is located at X = 5.8733". Both the inviscid and viscous wall solutions achieve a maximum stream Mach number of 1.9 at the nozzle exit. The inviscid wall solution indicates that in order to turn the flow at the plug tip, a shock is generated. Figure 15b shows corresponding Mach number contours associated with the viscous wall solution. As can be seen supersonic flow extends to a region near X = 36.

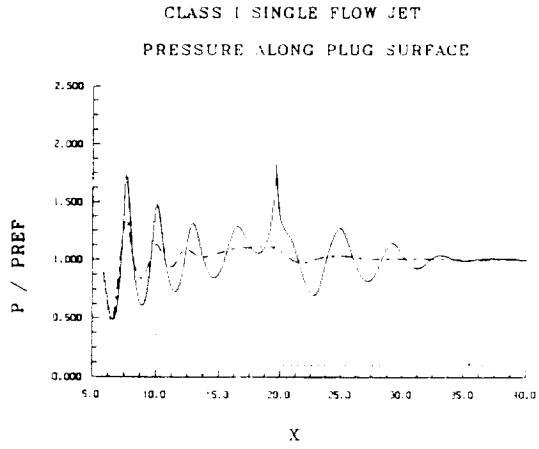

a - comparison of plug wall and centerline static pressures for slip and non-slip solutions.

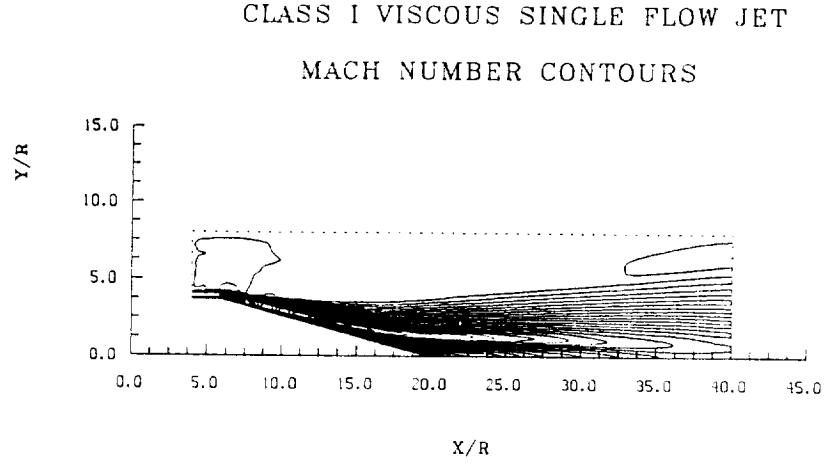

b - predicted Mach number contours.

Figure 20. PARCH code analysis of axisymmetric plug nozzle flow.

B3 - EVALUATION OF COMPRESSIBLE TURBULENCE MODELS

As described in section B1, accurate numerical prediction of supersonic shock containing flows is dependent upon the turbulence model installed in the code. Recently Sarkar (1990) has developed a new compressible turbulence model that shows an increase in the compressible turbulent dissipation, ε_{ij}, that would lead to a decreased growth rate with Mach number. From his results one sees that ε_{ij} only depends on Mach number,

$$\varepsilon_{ij}=\frac{2}{3}\bar{\rho}\varepsilon_s\left(1+\alpha_1 M_t^2\right)\delta_{ij}$$

$$\bar{\rho}\varepsilon_s(\text{Solenoidal Dissipation})=\bar{\mu}\left(\omega_i''\right)^2$$

A preliminary experiment was conducted in the NASA/LaRC JNL to examine the prediction. Using schlieren optical data, LDV and pitot tube measurements, the spread rate in the initial shear layer was measured. The results are shown in Figure 21. Except for the data at 305 K, the results are consistent with the Sarkar model. Future studies will investigate other Mach numbers.

Jet Stagnation Temp (Deg K)	dδ/dx
293 (Pitot)	0.22
305	0.08
810	0.17
925	0.17
1090	0.20
1090 (LDV)	0.19
1255	0.22
1255 (LDV)	0.21
1365	0.21
1430	0.19
1480	0.20
1580	0.22

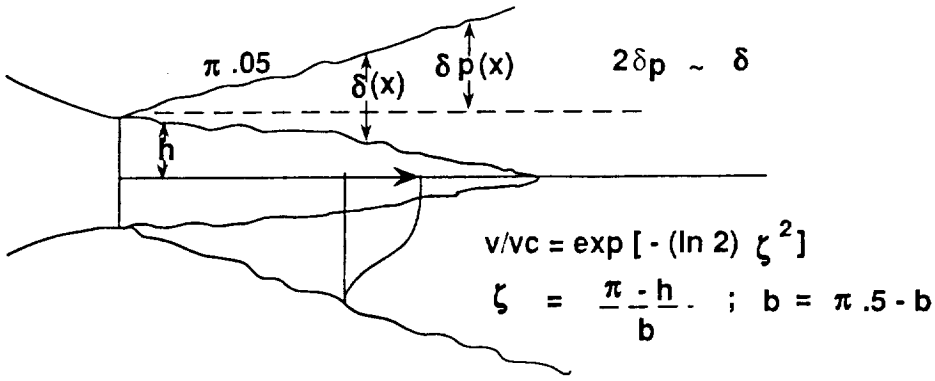

Figure 21. Examination of new compressible turbulent model.

C1 - NOZZLE GEOMETRY EFFECTS, CENTERLINE VELOCITY

For a shock-free supersonic jet, the amplitude of the emitted noise is a high power of the jet exit velocity. Therefore, any technique which rapidly reduces the plume speed without generating any additional noise will exhibit an acoustic benefit. Although round nozzle designs typically are used for turbine engines, a viable passive control of noise may be the use of asymmetric nozzles which promote rapid mixing thus lowering plume velocities and the associated noise. Possible geometries whould be those which can be designed shock-free to eliminate the presence of shock-associated noise.

An elliptic nozzle design method which produces a shock-free flow was developed by Seiner, Baty, and Kumar at the NASA-Langley Research Center. Two nozzles were constructed: Mach 2 of aspect ratio 3 and Mach 1.5 of aspect ratio 2. A comparison of the centerline velocity distribution is presented in figure 22 between the elliptic and shock-free axisymmetric nozzles. The axial dimension is normalized by the equivalent diameter of the nozzle. As is evident in the figure, the centerline velocity of the elliptic nozzles decays more rapidly than that of the round nozzles. One may expect a noise reduction through the use of this type of geometry.

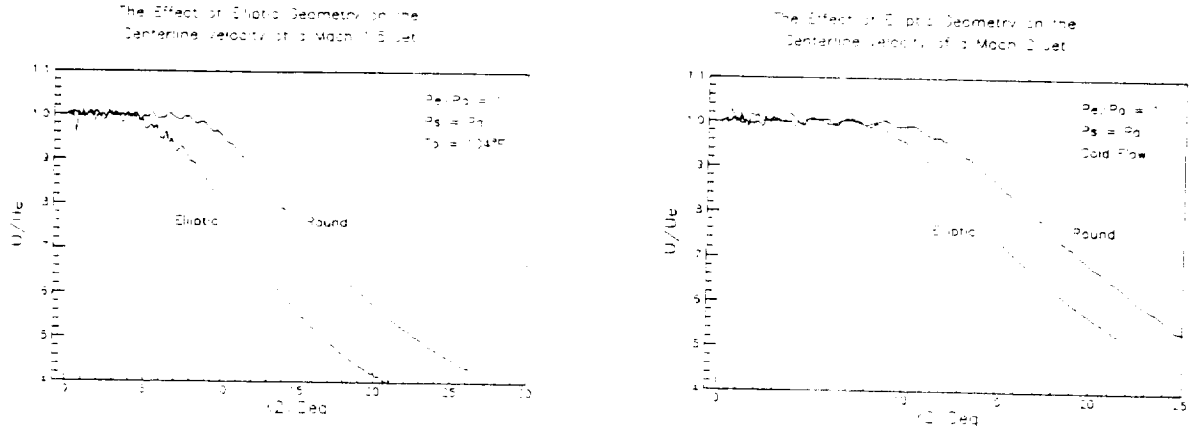

a - Mach 1.5 Jet

b - Mach 2.0 Jet

Figure 22. The effect of elliptic geometry on the centerline velocity distribution.

C1 - NOZZLE GEOMETRY EFFECTS, MOMENTUM THICKNESS

The momentum thickness has been used as a length scale of the initial turbulent shear layer (Ho, 1987). The initial azimuthal distribution of the momentum thickness controls the initial roll-up of shed vorticity while the axial distribution provides an indicator of the distortion of the jet column with downstream distance (Baty, 1990). The observed centerline velocity decay due to the elliptic geometry can be related to the asymmetric distortion of the major and minor axes momentum thickness. This distortion leads to enhanced mixing with the surrounding medium.

Figure 23a presents the axial momentum thickness distribution for the Mach 1.5 elliptic nozzle along both major and minor axes. Within the potential core (X/Deq < 5), the momentum thickness is essentially independent of major or minor axes and grows linearly, similar to a round jet. This indicates little azimuthal variation in the scales of initially shed vorticity. However, beginning approximately at the end of the potential core, the jet undergoes a large three dimensional distortion. The behavior of the Mach 2 elliptic nozzle is different as seen in figure 23b. The major axis momentum thickness increases at a greater rate with axial distance than does the minor axis momentum thickness. This is in contrast to the behavior of the Mach 1.5 elliptic nozzle. It is not known if this is related to the increased nozzle design Mach number or its increased aspect ratio. The minor axis momentum thickness of the round and elliptic jets are equal in the potential core region. Beyond the core region even the minor axis momentum thickness increases faster than the round nozzle.

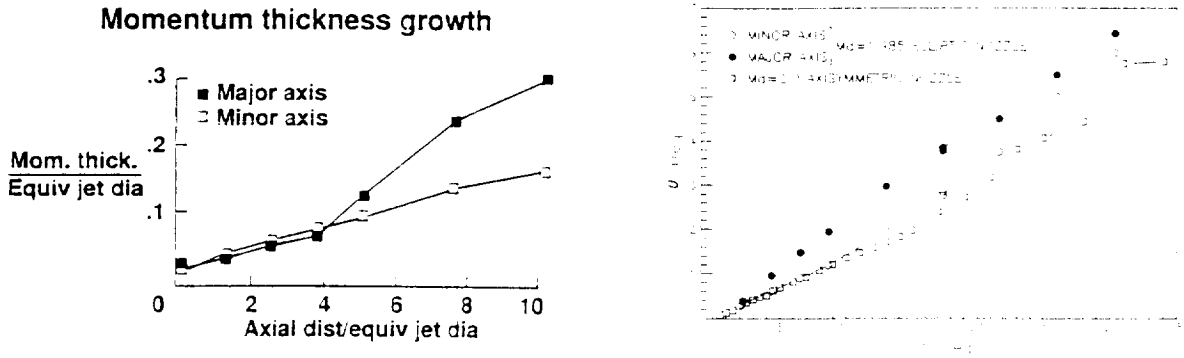

a - Mach 1.5 Jet

b - Mach 2.0 Jet

Figure 23. The axial momentum thickness distributions

C1 - NOZZLE GEOMETRY EFFECTS, SPECTRAL COMPARISON

The differences in the major and minor axes momentum thickness measurements for the Mach 1.5 elliptic nozzle would indicate the existence of a complex three-dimensional flow structure. This type of flow should have equally complex stability properties which would be manifest in the acoustic emission.

Figure 24 is a spectral comparison between the acoustic radiation of two azimuthal angles of the Mach 1.5 elliptic nozzle operating at a total temperature of 1160 R. Also included is a spectrum of the Mach 1.5 round nozzle corrected to the thrust of the elliptic nozzle. ϕ = 0 degrees is in a plane which contains the minor axis and the jet axis; ϕ = 90 degrees represents a plane containing the major axis and jet axis. The ψ angle is referenced to the nozzle inlet axis and a value of 128 degrees is the approximate direction of maximum overall acoustic emission. The data were acquired at approximately 127 equivalent diameters from the nozzle exit.

As is evident in the figure, a strong dependency exists between the spectral partitioning of acoustic energy and the nozzle geometry. Also, the acoustic field of the elliptic nozzle is azimuthally varying similar to the momentum thickness distribution. The overall sound pressure level of the round nozzle is 1 dB greater than the elliptic at ψ = 0 degrees and 4 dB greater than the elliptic at ψ = 90 degrees. Thus, geometry alone can yield acoustic amplitude benefits and possibly be used in the spectral redistribution of energy.

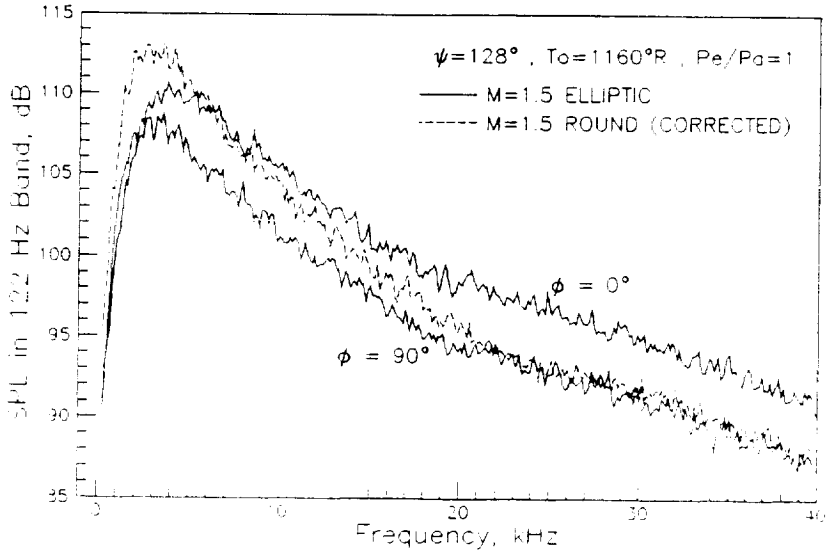

Figure 24. Spectral comparison of the acoustic emission from round and elliptic nozzle geometries.

C1 - NOZZLE GEOMETRY EFFECTS, PERCEIVED NOISE LEVEL

Due to the spectral differences created by nozzle geometry variations, the frequency-weighted perceived noise level would provide an important comparative metric for full scale applications. Acoustic data were acquired via a linear array for not only the Mach 1.5 round and elliptic geometries but also for an augmented deflecting exhaust nozzle (ADEN). The ADEN is a rectangular nozzle with parallel sidewalls and convergent-divergent flaps that differ in length in the nozzle exit plane. The data were scaled to 50000 lb of thrust at a sideline distance of 1476 feet and were propagated through a standard atmosphere using appropriate spectral corrections. These full scale conditions are representative of the requirements of the proposed high speed civil transport. ϕ is referenced as previously for the elliptic nozzle and for the ADEN ϕ = 0 degrees contains the nozzle's convergent-divergent plane.

Figure 25a indicates that for ϕ = 0 degrees, the elliptic geometry provides an acoustic reduction at the low ψ angles presented. The ADEN is not a three-dimensional contoured nozzle design and thus should contain shock noise which would increase the lower ψ angle amplitudes. Figure 25b shows an acoustic reduction for the elliptic nozzle as well as the ADEN when compared to the round geometry. Again note the presence of shock noise for the ADEN. This indicates the importance of identifying a passive noise control nozzle geometry which can produce a shock-free flow, similar to the elliptic nozzle tested.

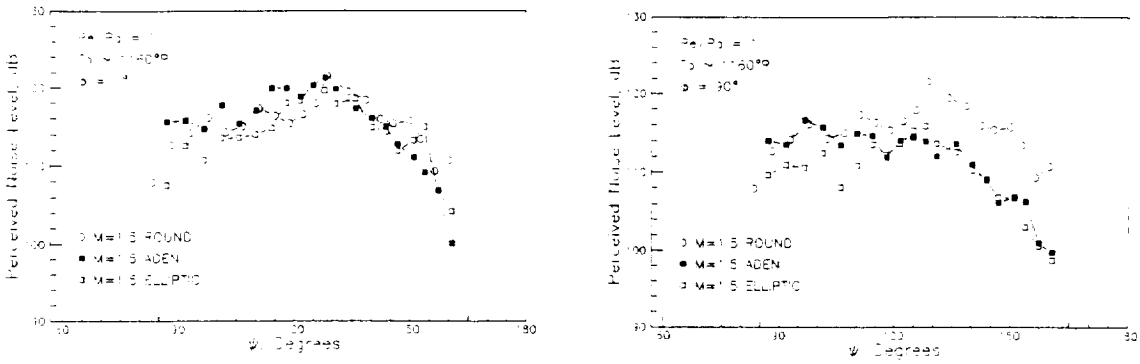

a - ϕ = 0 degrees

b - ϕ = 90 degrees

Figure 25. Comparison of the perceived noise level for various nozzle geometries scaled to a full scale application.

C1 - NOZZLE GEOMETRY EFFECTS, DESIGN MACH NUMBER

Figure 26 presents the azimuthal variation of the perceived noise level for both elliptic nozzles tested. The data is scaled similar to figure 25. The ψ angle corresponds to the approximate location of maximum acoustic emission. For flows which are shock-free, the data indicates a strong dependence of noise emitted on the velocity of the plume; i.e., greater exit velocities produce higher acoustic amplitudes. This dependence is evident for all azimuthal angles as indicated by the Mach 1.5 nozzle data for the two temperatures presented and also the Mach 2 data compared to the Mach 1.5 nozzle data.

The data also shows (similar to the previously presented spectra) that the acoustic amplitude is dependent on the azimuthal angle ϕ. In general, the perceived noise level decreases as ϕ approaches 90 degrees. This dependence represents another passive control method by which the nozzle orientation on a full scale engine can be manipulated to radiate the majority of the acoustic energy away from noise sensitive areas. It is important to note that because all nozzles are scaled to constant thrust, the lower temperature nozzle case should appear with smaller scaled noise because it is a higher mass flow nozzle.

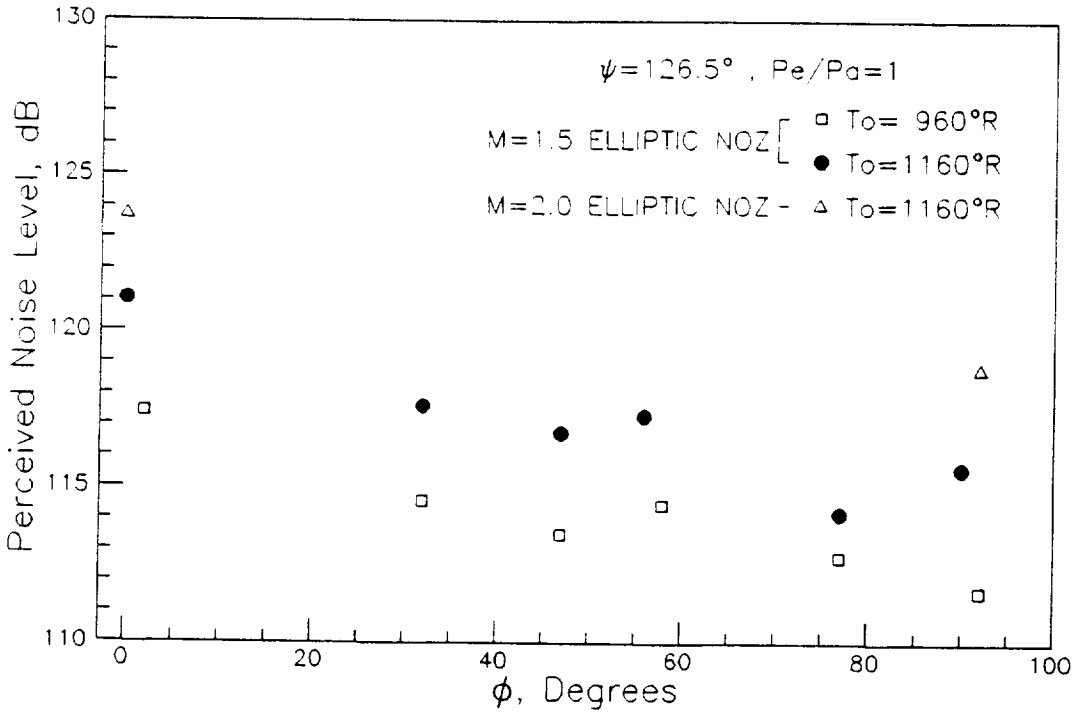

Figure 26. Comparison of the perceived noise level for the two elliptic nozzle geometries tested.

C2 - MULTIPLE JET INTERACTIONS

The HSCT suppressor nozzle, as currently envisioned, utilizes multiple hot high speed jets surrounded by afterbodies that promote rapid mixing with these jets. To show the types of interactions possible with multiple jet configurations, figure 27 presents a phased-averaged Schlieren photograph of unheated twin choked-tube nozzles (the strobe light is locked to the screech frequency for a given phase of the measured acoustic wave).

These nozzles were operated at a fully expanded Mach number of 1.32 where the dominant instability wave in the jet shear layer is a flapping structure (double helix). Generally, this type of large scale structure has no azimuthally preferred orientation. However, due to the mutual excitation of the jets, the flapping motion of both jets is now oriented in a plane containing the axes of both jets. This alters not only the azimuthal directivity of the screech noise but also promotes a more rapid mixing configuration as compared to a single nozzle. The potential thus exists for using the passive control feature of multiple jet interaction for acoustic benefits.

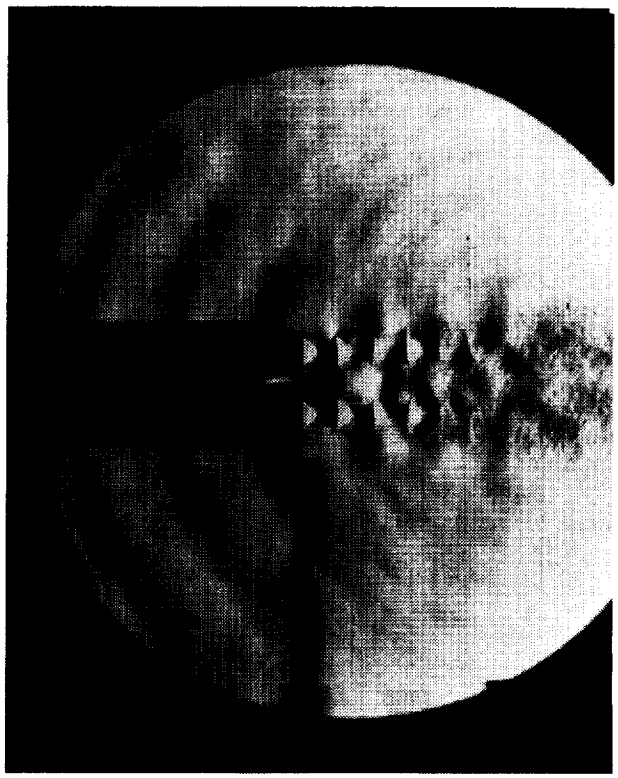

Figure 27. Phased-average Schlieren of twin choked-tube nozzles.

C2 - MULTIPLE JET INTERACTIONS

The envelope geometry for multiple jets in an HSCT application is either round or a low aspect ratio rectangular. The high speed jets emerge from geometries that are complex, but often driven by the geometric constraint of packaging in the envelope shape. The suppresor also makes use of an acoustically treated ejector that provides augmentation to the engine mass flow.

The elliptic jet geometry discussed previously shows that passive methods can be used to reduce noise. The properties of these non-round geometries, as exhibited by the deformation of the jet column (momentum thickness distribution), suggest that the orientation and location of the high speed mixer lobes is not arbitrary. A study of multiple jet interactions from a tri-axial configuration of nozzles (figure 28) is now underway at NASA Langley. The initial system uses a set of elliptic nozzles with varying aspect ratio combinations. The mechanism to support the tri-axial nozzle system permits location of the three nozzles to be arbitrarily rotated and positioned about a central axis. All elliptic nozzles are designed to be shock-free, so that an assessment of 3-D turbulent interaction can be studied without the influence of plume shocks. One cannot differentiate non-symmetric pressure gradients produced by shocks in the flow from that produced by turbulence.

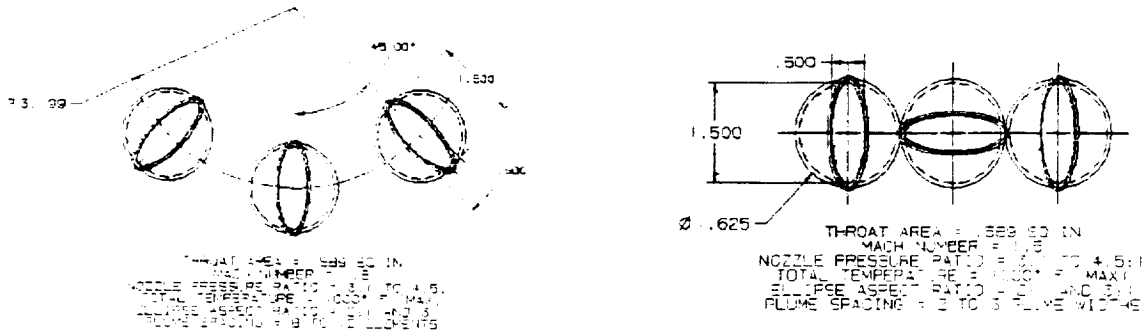

a - Simulated Suppressor Nozzle **b** - Interaction Mode

Figure 28. Example of tri-axial elliptic nozzle configuration.

C4 - ACTIVE CONTROL OF INITIAL JET SHEAR LAYER

The primary noise generation mechanisms of supersonic jet flows have been attributed to the presence of large scale structures in the shear layer. These dominant structures develop when small scale disturbances in the initial region of the jet grow in amplitude as they convect downstream. Therefore it may be reasonable to assume that by actively controlling initial shear layer instabilities, which have maximum growth rates, one can also control the noise emission.

C.M. Ho at University of Southern California is investigating practical methods for controlling the most unstable modes and their azimuthal energy distribution. These methods involve the use of sound, temperature, tuned cavities, and piezo-ceramic actuators to control the initial shear layer disturbances of axisymmetric and asymmetric nozzles operating in both the subsonic and supersonic regimes. Acoustic measurements have been made for a circular jet tested from the low subsonic to the transonic range. These measurements span the near field pressure fluctuations to the far field noise. The far field spectra presented in figure 29 indicate that for M=.2 to .35, the noise generated by large scale coherent structures in the thin shear layer dominates (high frequency peaks), while beginning at M=.4, the noise of the preferred mode dominates (broadband peak). The data will be compared to that acquired when various control methodologies are implemented.

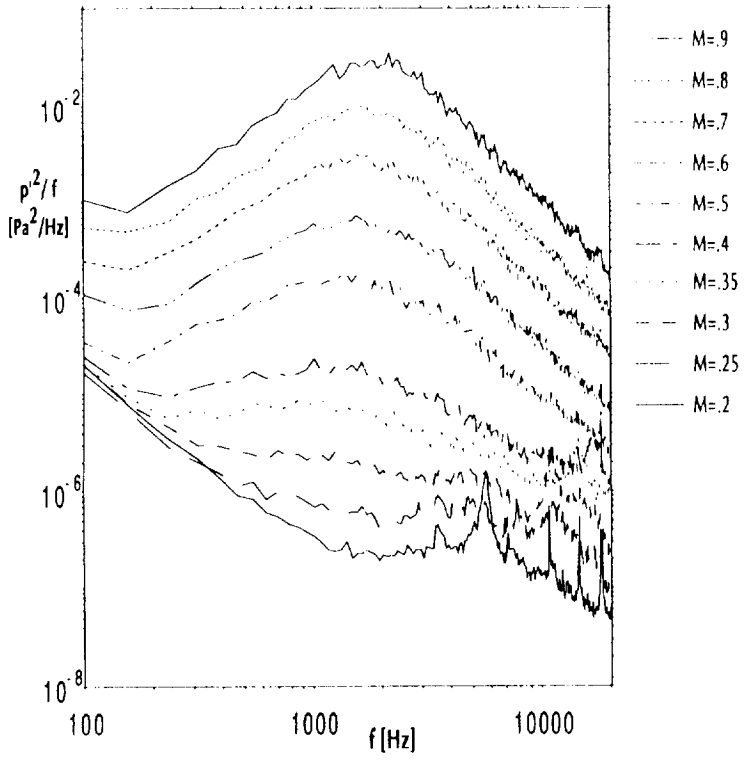

Figure 29. Far field spectra for an unheated circular jet operating subsonically.

D1 - SUPERSONIC INSTABILITY WAVES

An experiment is being planned in the NASA/LaRC JNL to verify the theoretical predictions of Tam (1990) on the occurrence of supersonic instability waves in high temperature jets where $T_s/T_a > 2.5$. The predictions of figure 30 show that with increasing jet temperature ratio, the Kelvin-Helmholtz instability wave amplitude decreases, but there is the appearance of a supersonic instability wave. These waves are produced by turbulence structure in the shear layer that convect supersonically relative to the local jet sound speed.

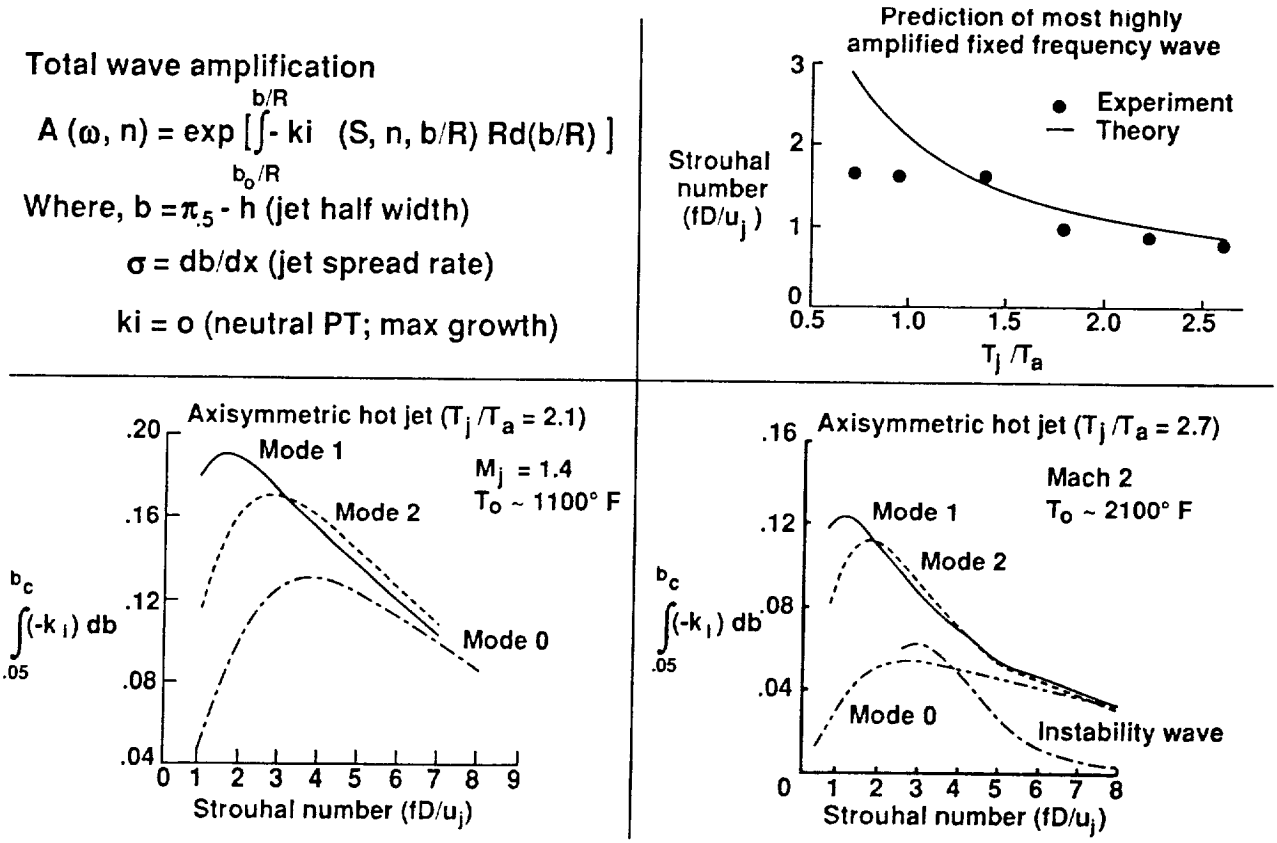

Figure 30. Instability waves in high temperature supersonic jets.

D1 - HIGH TEMPERATURE WATER COOLED NOZZLE

As a preliminary investigation into properties of hot supersonic jets and the questions regarding the directivity frequency and amplitude of the supersonic instability wave, Schlieren records were acquired from the hot Mach 2 axisymmetric nozzle shown in figure 31. This nozzle was designed to be shock-free at Mach 2 and a temperature of 2460 R. The nozzle exit diameter is 3.6 inches and is heated by the sudden expansion (SUE) burner in the JNL facility. This nozzle is water cooled and capable of being tested to 3000 R.

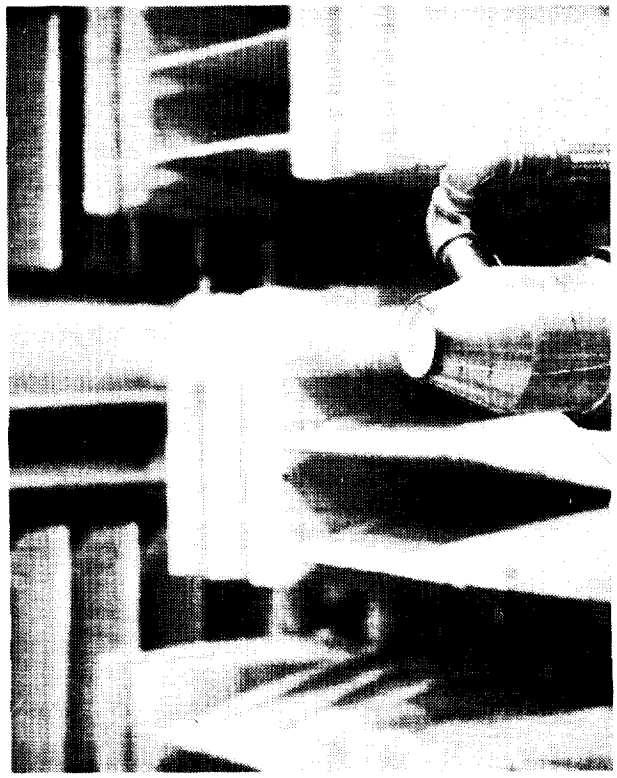

Figure 31. Mach 2 high temperature water cooled axisymmetric nozzle mounted in the JNL.

D1 - MEASURED AND PREDICTED MACH WAVE EMISSION ANGLE

Figure 32 illustrates a specific example between the measured and predicted Mach wave emission angle for a hot supersonic jet. In this example, the Mach 2 jet is being operated overexpanded at M_j = 1.5 and a temperature of 2466 R. Figure 32a shows the measured Schlieren data for this example. The Mach waves, which emerge from the edge of the shear layer, have wave normals that appear orientated 60 degrees to the jet axis. Based on Tam's (1990) large scale wave model, instability waves for this example will convect at 61% of the jet exit velocity. Based on this, the predicted wave angle is 59 degrees to the jet axis, as shown in figure 32b.

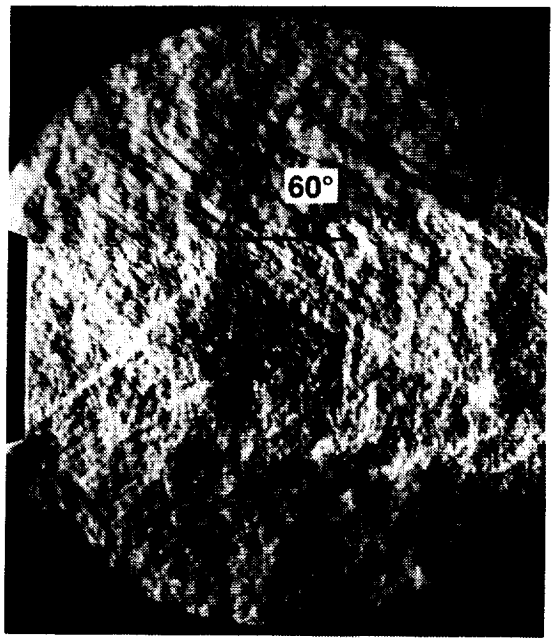

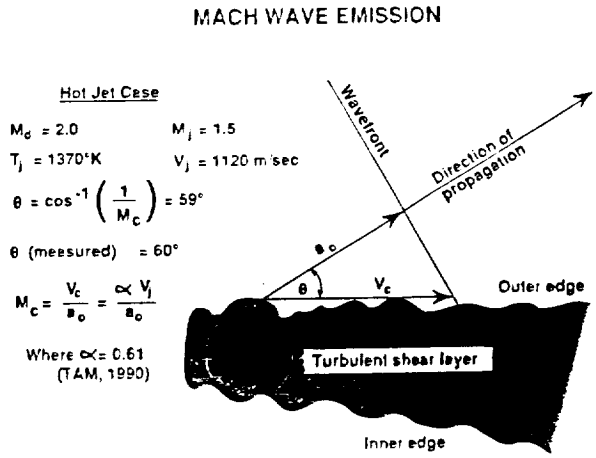

a - Schlieren of Mach 2 Jet

b - Predicted Mach Wave Angle

Figure 32. Measured and predicted Mach wave emission for a hot jet.

D2 - NON-LINEAR WAVE INTERACTIONS

Under certain operating conditions, shock-containing supersonic free jets have been shown to emit high amplitude narrowband acoustic signals referred to as screech tones. It has been suggested that the generation of this noise component is due to the interaction of the dominant large scale coherent structure in the turbulent shear layer with the shock cell system (Tam, 1986). Screech has been observed to be multi-modal, i.e. the jet exhibits different instability characteristics depending on the operating condition of the nozzle (Ponton, 1989). To better understand this noise mechanism, it is important to determine whether different screech modes are independent or interact non-linearly.

Two particular screech modes can be identified in the acoustic spectrum presented in figure 33a. These modes are the B and C modes, and are labelled accordingly. Also identified are the second and third harmonics of the C mode (2C and 3C) as well as narrowband processes occurring at the frequencies B+C and 2C-B. These latter two spectral components provided the impetus to perform a bispectral analysis on the data to determine if non-linear wave-wave interactions are occurring between the fundamental screech modes. This higher-order spectral technique reveals phase coherences between three frequencies satisfying the selection criteria $\omega_3 = \omega_1 + \omega_2$ indicative of a non-linear quadratic interaction (Ritz, 1987).

The bispectral analysis produced the auto-bicoherence contour plot shown in figure 33b. The diagonal lines are constant ω_3 lines and the two additional frequencies satisfying the selection criteria are obtained from the abscissa and the ordinate. As labelled on the plot, phase coherences are seen to exist between the C, B, and B+C frequencies as well as between the 2C-B, B, and 2C frequencies. This indicates that non-linear interactions are occurring and suggests that future acoustic models should encompass the observed source non-linearity.

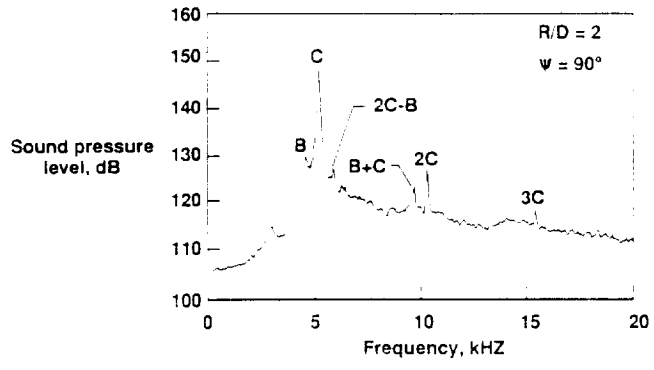

a - Auto-Spectrum

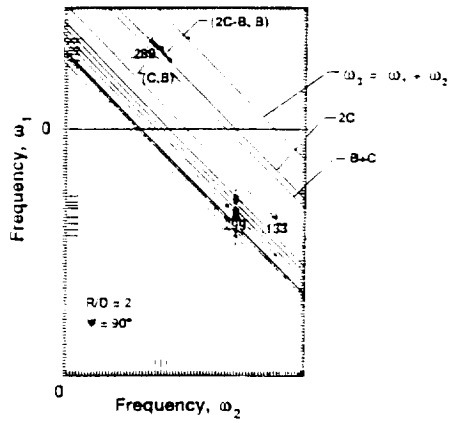

b - Auto-bicoherence Spectrum

Figure 33. Spectral analysis of the acoustic emission from an unheated round conical nozzle operating at $M_j = 1.44$.

D4 - PREDICTION OF NOISE FOR NON-ROUND JET GEOMETRY

The dominant sources of supersonic jet noise may be associated with the coherent structures in the jet mixing region, the jet's shock cell structure, and the interaction between these two phenomena. In this study the changes to the noise radiation associated with a change in the nozzle exit geometry is examined. An elliptic jet of aspect ratio 2 has been considered. The large scale structures in the jet are modelled as instability waves. These structures convect downstream with a velocity on the order of the jet exit velocity. For high Mach number or heated jets there is a direct coupling between the pressure fluctuations in the jet flow field and the acoustic field. This results in intense noise radiation. In the present study the characteristics of the large scale structures or instability waves are obtained from a solution of the compressible Rayleigh equation. In the region just outside the jet flow the pressure fluctuations are described in terms of Mathieu functions and modified Mathieu functions. These fluctuations are matched with the acoustic field using the method of matched asymptotic expansions. Figure 34 shows a typical far field calculation for the se_1 flapping mode. The two sections through the directivity pattern shown in figure 34 show (a) the variation with azimuthal angle ϕ for a polar angle of 30 degrees, and (b) the variation with polar angle θ for an azimuthal angle of 0 degrees. The decibel levels are in arbitrary units. Experimental data acquired at similar operating conditions, indicate the preference for axisymmetric structure and a wave direction at a steeper angle to the jet axis. Future calculations are being made to investigate stability properties of axisymmetric structure.

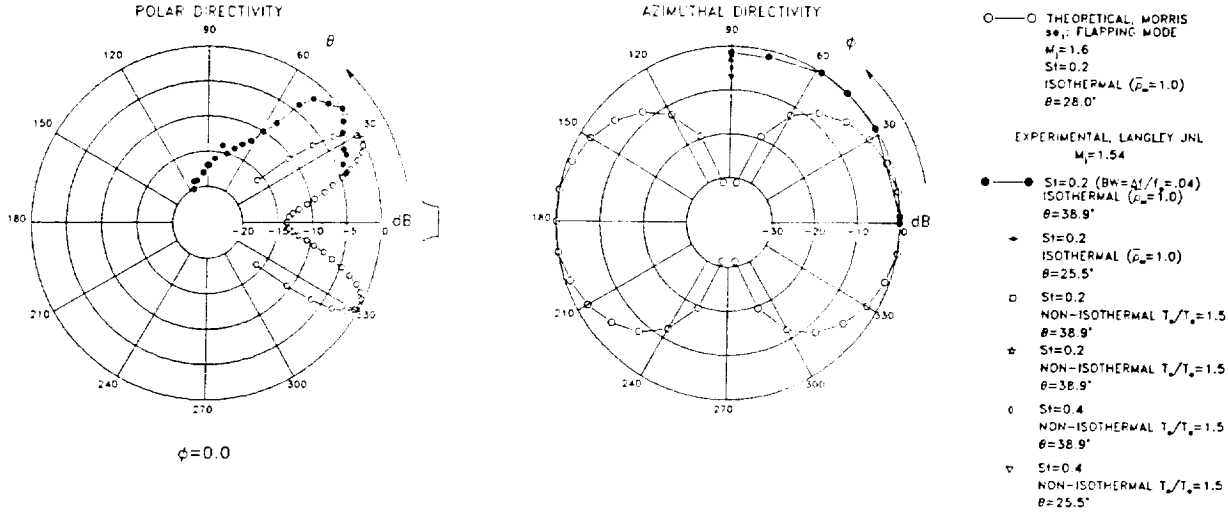

a - Polar Directivity **b** - Azimuthal Directivity

Figure 34. Far field directivity with azimuthal and polar angles.

D5 - LOW REYNOLDS NUMBER RESEARCH

The most promising theoretical developments in the prediction of supersonic jet noise involve the modeling of large scale turbulence structure (that produces a dominant portion of the radiated noise) with instability wave theory. Operation of model jets under low Reynolds numbers are achieved by exhausting the jets at low density (pressure) conditions in the low pressure anechoic chamber jet test facility (figure 35). Standard condenser microphones are used for the acoustic measurements and miniature hot-wire probes measure the turbulence structure in the jets. The unique feature of the latest measurements is that jets with helium/air mixtures are used to simulate heated jet conditions. This approach is a reliable way to evaluate the predictive capability of the analytical model. The first and simplest check is of the most unstable frequency of the primary jet instability (and radiated noise). Initial experiments have been performed with a jet operating at Mach 2, with a helium/air mixture that produces a velocity that is approximately 50% greater than the pure air jet. Shown in figure 36 are the acoustic spectra of air and an air/helium mixture jet. The most unstable frequency is shown to increase as the instability theory predicts it should. Numerous additional measurements are underway to explore these phenomena in more detail.

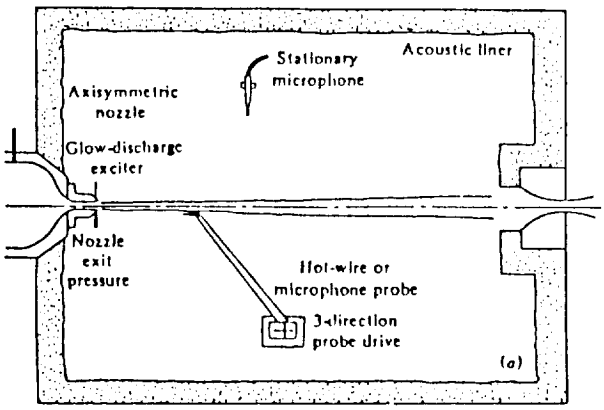

Figure 35. Low pressure anechoic jet test facility.

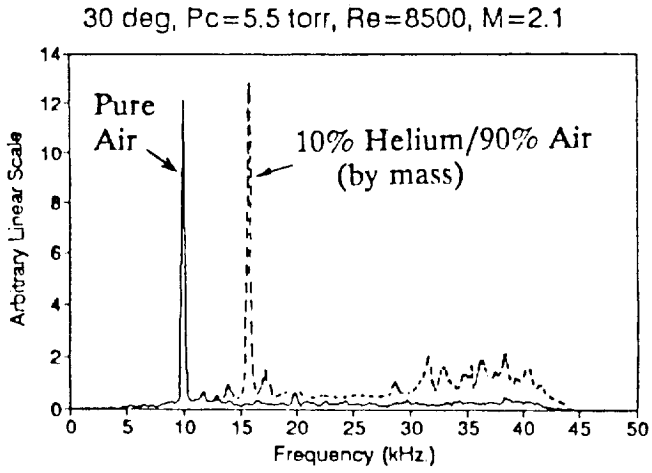

Figure 36. Acoustic spectra; M=2.1 air and helium/air jets.

REFERENCES

Baty, R.S., Seiner, J.M. & Ponton, M.K. 1990 Instability of a supersonic shock-free elliptic jet. AIAA Paper 90-3959.

Ho, C.M. & Gutmark, E. 1987 Vortex induction and mass entrainment in a small aspect ratio elliptic jet. J. Fluid Mech., 179, 383.

Ponton, M.K. & Seiner, J.M. 1989 The effects of initial jet exit conditions on plume resonance. AIAA Paper 89-1054.

Ritz, Ch.P., Powers, E.J. & An, C.K. 1987 Applications of digital bispectral analysis to nonlinear wave phenomena. ISSPA 87 Signal Processing, Theories, Implementations and Applications, 352.

Tam, C.K.W. 1990 Broadband shock associated noise of moderately expanded supersonic jets. J. Sound and Vib., 140, 55.

Tam, C.K.W., Seiner, J.M. & Yu, J.C. 1986 Proposed relationship between broadband shock associated noise and screech tones. J. Sound and Vib. 110, 309.

Weinstein, L.M. 1991 An improved large-field focusing Schlieren system. AIAA Paper 91-0567.